

The Si-Ge substitutional series in the chiral STW Zeolite Structure Type

Reus T. Rigo,^{1, a} Salvador R. G. Balestra,^{2, a} Said Hamad,² Rocío Bueno-Pérez,²
A. Rabdel Ruíz-Salvador,^{2, b} Sofía Calero,^{2, c} and Miguel A. Cambor^{1, d}

¹*Instituto de Ciencia de Materiales de Madrid (ICMM),
Consejo Superior de Investigaciones Científicas (CSIC),
Sor Juana Inés de la Cruz 3, 28049 Madrid, Spain.*

²*Department of Physical, Chemical and natural Systems,
Universidad Pablo de Olavide, Ctra. Utrera km 1, 41013 Seville, Spain*

(Dated: 6th July 2018)

The whole compositional range ($Ge_f = Ge/(Ge+Si) = 0$ to 1) of zeolite STW has been synthesized and studied by a comprehensive combined experimental–theoretical approach. The yield of zeolite goes through a maximum and then drops at the GeO_2 side of the series, following the inverse of the calculated free energy curve. The unit cell generally expands, roughly linearly, as the Ge_f increases, but a notable resilience to expansion is observed at the high silica side. This can be attributed to the more rigid character of SiO_2 and the ability of Ge units to deform. Density functional theory calculations provide a new assignment of the previously controversial ^{19}F MAS NMR resonances for occluded fluoride, which is based not only in the number of Ge atoms in the double-4-ring units but also on the way they are associated (namely, no Ge, isolated Ge, Ge pairs or closed Ge clusters). While we found an overall good agreement between the experimental and theoretical trends in preferential occupation by Ge of different crystallographic sites, the theoretical models show more sharp and abrupt tendencies, likely due both to limitations of the approach and to kinetic factors that allow metastable configurations to actually exist.

I. INTRODUCTION

Zeolites find an extraordinarily wide commercial applicability,[1] and this in turn fosters further research aimed to the synthesis of zeolites with new structures and compositions.[2] Among the many factors determining the phase that crystallizes in a zeolite synthesis,[3] the organic structure directing agents (SDA),[4] fluoride anions,[5] and framework elements other than Si and Al (Ge, Zn, Be, Ga ...) may afford the discovery of new zeolite structures.[6] In particular, Germanium, specially when used together with fluoride, tend to produce structures with double 4-ring units (D4R).[7–9] Despite the low stability of Ge-zeolites upon both calcination,[10] and hydrolysis by ambient moisture of the calcined materials,[11] the discovery of new Zeolite Framework Types (ZFT),[12] even if unstable, is still of interest. In fact, the weakness of Ge-zeolites has been advantageously used to derive new materials from them through the assembly-disassembly-organisation-reassembly strategy (ADOR), which has so far produced several interesting zeolites that are, in addition, more stable than the parent one.[13–16] These derived zeolites may be 'unfeasible' to obtain by the conventional hydrothermal routes, adding interest to Ge-zeolites.[17] On the other hand, Ge-zeolites may be stabilized by postsynthetic treatments by substituting Ge by Si or Al.[11, 18–20] Finally, unstable but structurally

interesting zeolites discovered by using Ge, such as the chiral zeolite STW,[21] can become a target for the synthesis of more stable materials with the same structure, as was the case for the STW pure silica version, HPM-1.[22, 23]

STW was first realized as a germanosilicate.[21] Its interest relies on its chiral nature and the presence of a helicoidal medium pore channel. Every single crystal is homochiral but standard synthesis procedures using achiral organic SDA are expected to yield racemic conglomerates.[21–23] However, very recently it has been possible to prepare enantiomerically enriched scalemic conglomerates by using an enantiomerically pure chiral dication, and the materials proved to yield small but significant enantiomeric excess in both asymmetric catalysis and adsorption processes.[24] These syntheses produced germanosilicate and aluminogermanosilicates, but recent studies suggest homochiral STW silica phases may as well be possible.[25] These silica zeolites are expected to be not only much more stable but also more amenable to selective separations, since the larger flexibility of GeO_2 frameworks appears to be detrimental to chiral recognition.[26] Here we report that substitution of Si by Ge in the chiral D4R-containing zeolite structure STW can be attained for any value of the Ge molar fraction ($Ge_f = Ge/(Ge+Si)$). By combining experiment and theory we have been able to get significant insight into that system, particularly on the energetics of the zeolite, the unit cell expansion, which is buffered at the low Ge_f side, the previously controversial assignment of the fewer than expected ^{19}F MAS NMR resonances, and the differential occupation of crystallographic sites as Ge_f increases. This insight is expected to be of general interest within the field of Ge-zeolites and their flourishing de-

^a These two authors contributed equally to this work.

^b Corresponding autor:rruisal@upo.es

^c Corresponding autor:scalero@upo.es

^d Corresponding autor:macambor@icmm.csic.es

rived strategies to develop new materials.[13–17]

II. EXPERIMENTAL

A. Synthesis

All the zeolite syntheses were done using equimolar amounts of hydrofluoric acid and 2-ethyl-1,3,4-trimethylimidazolium (2E134TMI) hydroxide. 2E134TMI was synthesized as iodide salt and exchanged to the hydroxide form as previously reported.[27] The synthesis mixture was prepared by adding (if required) first tetraethylorthosilicate (TEOS, 98% Aldrich) and then (if required) germanium dioxide (99.998% Aldrich) to a concentrated solution of 2E134TMI hydroxide. The mixture was stirred at room temperature allowing evaporation of ethanol (if TEOS was used) and water, until the desired composition was reached. Evaporation was monitored by weight. Then, hydrofluoric acid (48 wt%, Sigma–Aldrich) was added to the gel and stirred with a spatula for approximately 15 minutes. The obtained gel was transferred to Teflon vessels inside stainless steel autoclaves, which were heated in an oven at a temperature of 175 °C while tumbling at 60 rpm. At preselected times (generally close to 24, 48, 144 and 240 hours), the autoclaves were removed from the oven and quenched and the product filtered on paper or centrifuged, washed with deionized water and dried at 100 °C. The final composition of the gel was: $(1-x)\text{SiO}_2 : x\text{GeO}_2 : 0.5 \text{ 2E134TMI} : 0.5 \text{ HF} : 4\text{H}_2\text{O}$, where $x = \text{Ge}/(\text{Si} + \text{Ge})$ is the molar fraction of germanium oxide, which will be expressed in the following as Ge_f .

B. Characterization

Power X-ray diffraction was performed using a Bruker D8 Advance diffractometer, with Cu K_α radiation in the 3.5–45 ° 2θ range. The unit cell of HPM-1 samples with varying Ge_f were refined by a least squares regression procedure using the program UnitCell and 16 reflections uniquely indexed in space group P6_122 , covering the 8–30 ° 2θ range.[28] Synchrotron X-ray powder diffraction data were collected at the SpLine BM25A at the ESRF, Grenoble, in capillary mode (0.8 mm diameter) using monochromatic radiation ($\lambda = 0.56383 \text{ \AA}$) for the samples synthesized with $\text{Ge}_f=0.4, 0.6$ and 1.0 . Rietveld refinement was performed using GSAS,[29] under the EXPGUI graphical interface.[30] C,N,H analyses were performed with a LECO CHNS-932 instrument. Ge and Si chemical analysis were performed by Inductively Couple Plasma–Mass Spectrometry (ICP-MS) using an ICP-MS NexION 300XX equipment. ^{19}F , ^{29}Si , ^1H and ^{13}C MAS NMR experiments were recorded on a Bruker AV 400WB, as described elsewhere.[31] Field emission scanning electron microscopy (FE-SEM) images were obtained with a FEI NOVA NANOSEM 230 without metal

coating. Thermogravimetric analyses were obtained with an SDT Q600 from TA Instruments at a heating rate 10 ° C min^{-1} under an air flow of 100 mL/min.

C. Theoretical methodology

The STW framework has a large unit cell with sixty tetrahedral sites with five symmetrically distinct sites.[27] This conduces to massive amounts of symmetrically unique Si-Ge configurations for each Ge content by unit cell in the interval from 4 to 56. To deal with this, we employ a recently developed method that evaluates the energy of the system using an effective Hamiltonian (EH, see Supplementary Information).[32, 33] The EH was parameterized using the lattice energy of the pure SiO_2 STW zeolite and the substitution energies for 1 to 4 Ge atoms by unit cell computed with interatomic potentials. Explicit calculations of the lattice energy are computed for the whole set of possible symmetry non-redundant configurations up to 3 Ge by unit cells. The selection of these configurations was achieved with the Site Occupancy Disorder (SOD) program,[34] which allows to reduce at least by one order of magnitude the computational cost by discarding the redundant configurations. Details of the number of configurations used for each Ge content are collected in the Supplementary Information (see Table S1).

For four Ge per unit cell, 40890 inequivalent configurations appear, which represented a heavy computational cost. We noted during the energy minimization with lower Ge content that the convergence of the calculations is rather slow, as compared to aluminosilicate zeolites due to the presence of multiple local minima on the total potential energy surface, which we identify as originated by the larger flexibility of the solids associated to the presence of Ge. Therefore, the lattice energy of ca. 3.68 % of the 4-Ge configurations were explicitly computed by standard atomistic methods and the remaining 96.31 % by using the EH. The selection of this 3.68 % was achieved by considering those relevant configurations having three neighbour Ge atoms and the fourth one as first or second neighbour of one of those three. A more spread distribution of Ge atoms causes a lower effect on the local structure and can therefore be accurately described by the EH. Once the EH was parameterized, it was used to compute the lattice energy of each configuration (see Equation S7). The atomistic calculations were performed with the GULP code,[35] using Sastre and Gale interatomic potentials,[36] which have been used in the past to predict preferable occupation of Ge in D4R.[37, 38] Short-range Buckingham potential was evaluated within a cut-off of 16 Å, while the long-range Coulomb potential was calculated by the Ewald method.[39] Energy minimization was performed with the BFGS minimizer,[40] switching to RFO method after a suitable progress of the structural relaxation to remove the existing imaginary vibrational modes, if any,

and therefore providing true energy minima structures. This procedure has been proven to be particularly useful for modelling zeolitic materials.[41–43]

To reduce the size-effect contribution in the error of averaged observables we have designed an ensemble of special quasirandom structures (SQS's),[44] that mimic the average in composition of the calculated structures and radial correlation functions of optimised structures for each molar fraction. The generation of these structures take into account the free energy of the unit cell for each Ge content and correlation functions. SQS's have been extensively used in substitutionally random A_xB_{1-x} solids in the past,[44–46] but never in nanoporous crystals, to our knowledge.

The use of the EH and SQS's allowed us to evaluate the free energy of formation of the zeolites in the complete range of Si/Ge content, by appropriate Boltzmann weighing and considering also the configurational entropic contribution. For each given number of Ge atoms per unit cell, we selected the 50 lowest energy configurations for the theoretical estimation of the structural features. They were subject to interatomic potentials full lattice energy minimizations using the same type of calculations described above. Since we are interested in understanding the behaviour of the cell parameters and volume as a function of the Ge molar fraction and the size constrains of our calculations leads to small variations of the hexagonal symmetry, we renormalized a and b parameters. For this, we take for each configuration the cell volume invariant given by the energy minimization, as well as the cell parameters and force the cell angles to be $\alpha = \beta = 90^\circ$ and $\gamma = 120^\circ$, while recalculating a and b cell parameters.

An open source Fortran 2003 code for the manipulation and generation of the most probable structures (using the effective Hamiltonian analysis and the special quasirandom structures theory) is available at https://github.com/salrodgom/ising_cation_3D_nanoporous.

Density Functional Theory calculations were conducted to compute the ^{19}F -NMR chemical shift, using the linear response method.[47, 48] It is known that calculations of chemical shifts computed using the PBE functional,[49] might differ from the experimental measured values in cases where the covalency of the system is significant,[50–53] with differences as high as 80 ppm.[54, 55] Due to the large size of our system, we cannot perform the types of the electronic structure calculations with hybrid DFT functionals that would solve this issue. We then have to use PBE, in spite of quantitative agreement between experimental and computed chemical shifts is not expected, as we have a system with varying degree of covalency of the Ge–F interactions at the different SiGe–F environments. However, we do expect to use the computed values to identify the existence of distinct resonance peaks. Due to the large number of Ge substitutions that we will study, a wide range of resonance peaks is expected to appear, and we will try to assign

the experimentally observed peaks using the theoretical chemical shifts.

Regarding the generation of the Ge-substituted zeolite for the NMR calculations, as mentioned above, the number of possible non-equivalent configurations is too high. Besides, the geometry optimization of each configuration is computationally expensive, due to the combination of a large size of the zeolite, Pulay forces (inherent to the plane wave DFT calculation of periodic solids with varying cell volume), and the large structural flexibility caused both by the zeolite framework and the presence of extra-framework species (fluor counteranions and template cations). As a consequence, we manually created eight zeolite structures, which allow us to include all possible Si-Ge distributions (about 20) within the D4R units. Since STW zeolite has 6 D4R cubes by unit cell, by constructing eight zeolite structures we ensure that each Si-Ge D4R distribution was considered at least two times, which is useful to validate transferability of the results and to increase the size of the sampling space to provide more accurate estimation of the errors. Several works report the calculation of the chemical shift using non-periodic, isolated D4R units, having the F atom inside. It is assumed then that the chemical shift is a local property, which depends only on the composition and Si-Ge distribution of a given D4R cube, and on the resulting chemical environment of the F atom. Details of these structures are provided in the supplementary information.

All DFT calculations were performed with the VASP program,[56–59] using the PAW potentials,[60] the PBE functional connected to the D3 van der Waals potential,[61] and 900 eV cut-off for both the geometry optimization and the NMR data calculation. Since the calculation of chemical shifts requires the computation of magnetic energy levels separated by very small gaps, very tight minimization criteria for the structural relaxations are needed. The calculations of the chemical shift on STW structures optimized using 600 eV cut-off did not converge in six out of eight structures, which caused the need to perform very expensive energy optimizations, with 900 eV cut-off. All calculations were performed with the gamma point only, due to the large size of the unit cell.

III. RESULTS AND DISCUSSION

A. Synthesis

The use of 2E134TMI and fluoride allows the synthesis of HPM-1 (STW) zeolites in the whole 0-1 range of Ge_f molar fractions (see Table S2). The robustness of this type of synthesis that combines the structure directing effects of both 2E134TMI and fluoride ions is revealed not only by the full Si-Ge substitutional range attainable but also by the fact that STW is the only zeolite that crystallized within a relatively

wide range of crystallization times. This clearly reveals the superior structure-directing effect of 2E134TMI compared to the original organic SDA (diisopropylamine), which produced a mixture of phases,[21] or a more recent SDA (N,N-diethylethylenediamine) which produced a pure STW phase in a limited range of conditions (particularly regarding the Ge_f compositional range).[62] For another recent SDAs based in the imidazolium ring (pentamethylimidazolium), only the synthesis of either pure silica STW or of intermediate germanosilicates and germanoaluminosilicates have been so far reported.[23–25] We also point out that the synthesis of pure GeO_2 -STW had never been described before.

The combined structure-directing ability of 2E134TMI and F^- is likely helped up to some extent by the tendency of Ge to produce zeolites containing D4R (a structure-direction tendency shared with fluoride). However, and somehow surprisingly, the crystallization of the pure Ge-end member appears to be the less favorable one within the series, since only in that case we observed noticeable deviations from the noted crystallization of STW (see last five entries in Table S2): at short times (27 hours) we collected no solids by filtration or centrifugation, while at long times (over 100 hours) a dense quartz-like phase, and latter an argutite-like phase, started to compete. We also observed some reproducibility problems at $Ge_f=1$, since in two different runs we obtained either a very small yield of pure HPM-1 at 113 hours or HPM-1 with some quartz-like GeO_2 in a higher yield at 96 and 102 h.

At the more Si-rich side of the series, STW is the only crystalline phase produced and its crystallization markedly accelerates when Ge substitutes for Si even in very small fractions (compare entries 1, 5 and 9 in Table S2). It is interesting that, for any of the crystallization times producing STW, the yield of zeolite goes through a maximum as Ge_f increases and then decreases significantly, so that the value for the pure germanate material is much lower than for the pure silicate end member, Figure 1. The oxide-based yield shows even stronger differences: the value for the Ge-end member is less than half that of the Si-end member and less than a quarter of the maximum at $Ge_f \approx 0.4$.

We note (see Figure S1 in the Supporting Information) that the relationship between the Ge molar content in the gel and in the zeolite is almost linear, but there are small deviations that perfectly match a non-linear fit to a 3rd order polynomial. These deviations are however small in magnitude and cannot explain the observed change in yield. Hence, in order to get a deeper understanding of the factors that influence the observed volcano-type curve of the synthesis yield, we calculated the free energy of formation of the zeolite, which is plotted in Figure 1 as a function of the Si/Ge molar fraction. As shown in the figure, the yield curve has an asymmetric shape and is in close agreement with the inverse of the free energy of formation predicted by the atomistic modelling, i.e. the position at which the yield reaches the maximum value

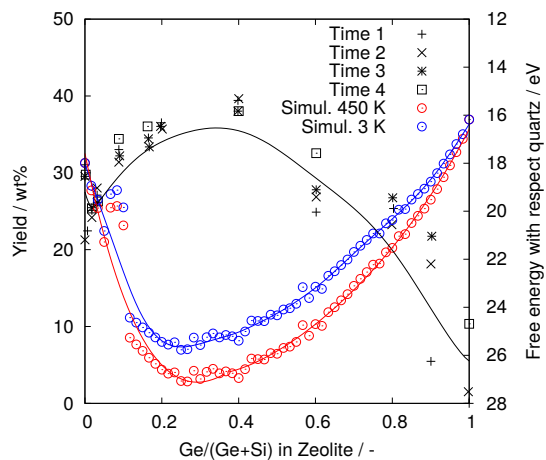


Figure 1. Yield of solids as a function of the Ge molar fractions in the zeolites (black dots). At any given Ge_f different data markers refer to different crystallisation times. Bézier black curve fitted from experimental points is shown in the figure as a guide to the eye. Free energy as a function of Ge_f at 450 K and 3 K, red and blue circles, respectively. Red and blue solid lines represents non-linear fittings of a potential function.

matches the minimum of the free energy curve. Thus, the observed change in yield responds to the change in free energy, as expected. It is also worth noting that the entropic contribution does not affect in a significant way the shape of the free energy curve, since the simulation results are very similar for temperatures as different as 3 and 450 K.

B. Characterization

The powder XRD patterns of the STW samples, Figure 2, display clear changes in the positions of the different reflections as the composition changes. This is, in principle, as expected because of the Ge substitution for Si and the different size and different T-O lengths of Si and Ge. There are abundant examples in the literature of close to linear changes of unit cell parameters as a function of T-atom substitution,[63–65] although at least one exception showing a reversal of the expected trend also exists.[66]

In the case of Si,Ge-STW, the overall trend is the expected expansion as the Ge fraction increases and the correlation is indeed close to linear, specially for $Ge_f > 0.2$, for both the unit cell edges size and volume. However, a careful inspection at the high silica side of the series shows little, if any, noticeable change in the bottom five traces of Figure 2. In fact, the refined unit cells do not change appreciably for small substitutions of Si by Ge ($Ge_f < 0.2$). As seen in Figure 3 the overall increase in a , c and V from the pure silica to the pure germania end members is of around 4.4, 3.3 and 12.6%. However, in the Ge_f range from 0 to 0.1 there are essentially no

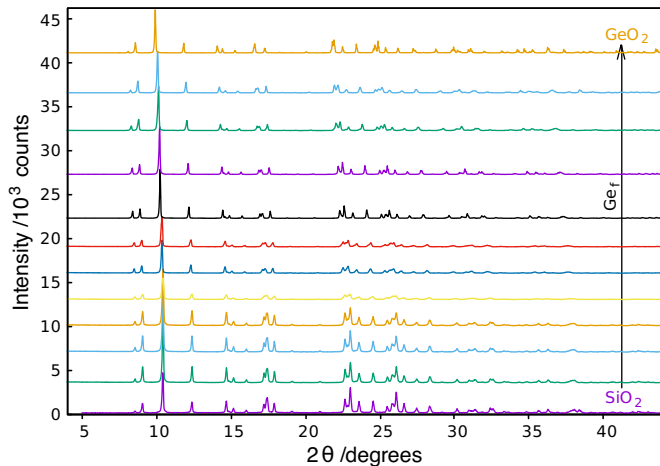


Figure 2. Powder XRD of the (Ge,Si)-HPM-1 series with varying germanium molar fractions in the gel (from bottom to top) $Ge_f = 0.00, 0.009, 0.019, 0.032, 0.09, 0.167, 0.20, 0.40, 0.60, 0.80, 0.90$ and 1.00. All the samples were crystallized at 175°C for 144 hours, except the top one, pure GeO_2 -HPM-1, which was crystallized for 113 h.

changes, instead of the expected increase in unit cell to around $a = 11.95\text{ \AA}$, $b = 29.78\text{ \AA}$ and $V = 3690\text{ \AA}^3$ if the overall trend were followed.

We propose that, since the $[GeO_{4/2}]$ tetrahedron is larger but also more flexible than the $[SiO_{4/2}]$ tetrahedron, small amounts of Ge can enter the framework without significantly altering the unit cell size. This buffering effect appears to occur in the 0-0.1 range and contrasts with the relatively large changes in the ^{29}Si and specially ^{19}F spectra of the same samples (see below). This could be related to a preferential sitting of one Ge atom in each D4R in this Ge_f range, see below. In contrast, in Ge-MFI, lacking D4R, Kosslick et al. found a significant increase in the cell parameters in the 0-0.13 Ge_f range.[67]

In order to understand the reasons for the observed changes in cell parameters and volume, we made use of lattice energy minimisation based geometry optimization, which give us an atomistic insight into the system, in direct connection with the local structure. There are some limitations to the accuracy that our simulations can provide, associated mainly to the use of force fields, and the non-inclusion of factors such as temperature and the presence of SDAs in the structure. But despite those limitations, we found a good agreement between simulation and experimental data (see Figure S2), which gives us confidence in the atomistic behaviour of the simulated system. To extract the relevant information, we plot the changes of T-T and T-O distances, as well as T-O-T angles, as a function of the Ge content. Since the Ge_f in the zeolite was close to that in the gel but not completely identical, we performed a non-linear fit of the data (see Figure S1) and represent the experimental cell values as

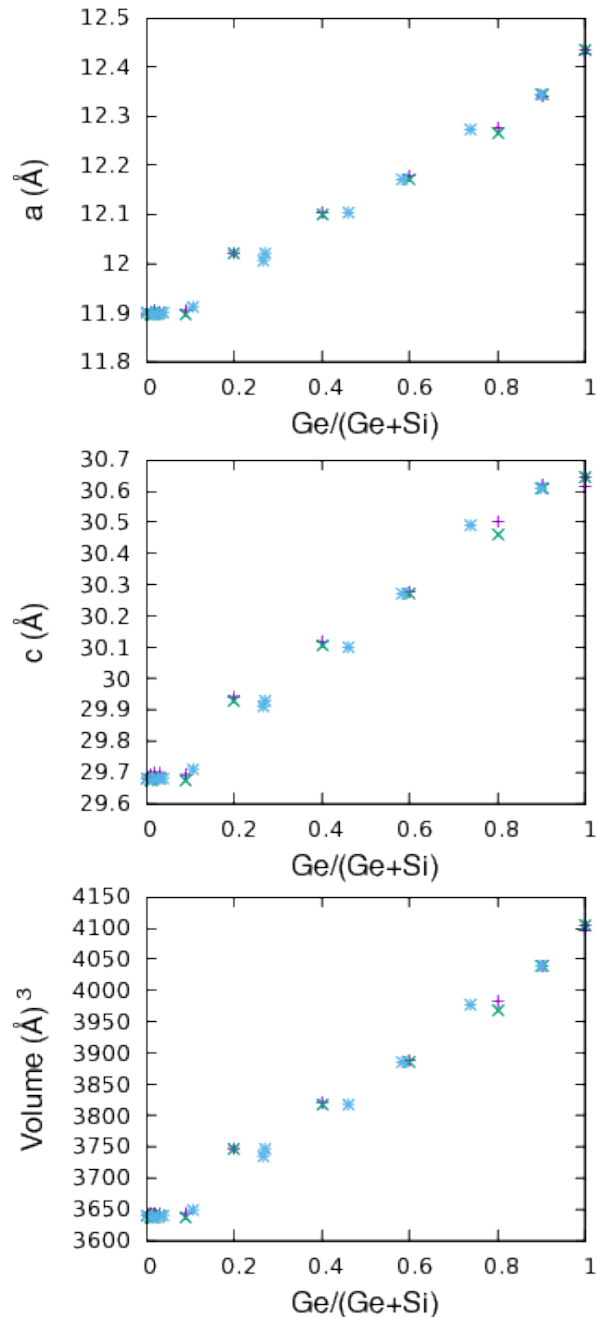


Figure 3. Variation of the unit cell edge a (top), the unit cell edge c (middle), and the volume V (bottom) of (Ge,Si)-STW as a function of the Ge fraction in the gel. Purple + and green x markpoints correspond to samples crystallized for 24 and 144 hours, respectively. Blue asterisks correspond to Ge_f experimentally measured by ICP.

a function of the calculated Ge_f in the zeolite. As we can see in Figure 4, the fact that, at low Ge contents, the cell volume remains constant (as observed in Figure S2), can be explained by the ability of a Ge tetrahedron to adapt to local deformations. In order to better understand the curves shown in Figure 4, we remind that the original

unit cell has 60 Si atoms, so that the fully Ge-substituted system is achieved after the 60 additions represented by the 60 crosses of the figures. The first cross corresponds to the substitution of just one Ge atom. It is noticeable that, at very low Ge contents, both distances (Ge-O) and angles (O-Ge-O and Ge-O-T) show singularities, which can be understood as follows. The introduction of only one Ge in each of the six D4R cubes is easily accommodated by the structure, as the effect of the enlarged T-O distance is compensated by reducing the T-O-T angles, as shown in Figure S3. It is important to note that the presence of a F atom nearby the Ge atom causes larger distortions than those expected by the sole effect of the introduction of a Ge atom. While exploring the conformational space towards the global minimum energy, we noticed the presence of multiple local minima along with the deformation of the Ge bearing tetrahedra, indicating the presence of a complex potential energy surface. The small relative depth of the energy wells served as an indication of accessible metastable phases and of the probability of transitions, which suggests dynamic flexibility behavior, in agreement with previous findings.[26, 68, 69] This suggests that modelling the structural features of Ge containing zeolites, even with a static view, provides means for predicting the flexibility, if any, of these materials. The addition of a second Ge atom in a D4R cube brings a large asymmetry into the local structure around the Ge atoms, since only one of the two Ge atoms is in close contact with the F atom (at ca. 1.82 Å), while the other is further away (ca. 2.75 Å). As a result, the former Ge atom behaves, from a local structure point of view, similarly to an isolated Ge-F pair, and the later behaves like an isolated Ge atom. We thus anticipate that the resilience to modify the cell upon a small extent of Si substitution by Ge may be a rather general behaviour for D4R-containing zeolites (we could not find relevant crystallographic data in the literature for this low Ge_f range, though).

The infrared spectra of a series of as-made STW zeolites prepared from gels with different Ge_f are shown in Figure S4. Apparently, the overall effect of the presence of Ge is to cause a new set of vibrational bands at lower wavenumbers, rather than simply redshifting the bands.

Figure S5 shows that as the Ge_f increases the crystal habit changes in the sense of gradually reducing the prismatic faces. Thus, the 'double tip pencil' habit (i.e. hexagonal prisms ending in hexagonal pyramids) characteristic of pure silica and very high silica HPM-1 almost completely disappears for $Ge_f \geq 0.2$, which consists of hexagonal bipyramids.

The thermogravimetric analyses of HPM-1 solids prepared at different Ge_f ratios are provided in the supplementary information (Figure S6). As the Ge fraction increases the weight losses decrease, as expected for the larger atomic mass of Ge compared to Si. Further, the temperature of the main weight loss also increases and, for the higher Ge_f values, several weight gain events

are clearly observed (starting mainly around 700 °C and again around 900 °C), both effects likely resulting from the complex nature of oxidation–reduction processes that Ge-containing zeolites typically undergo (notably including framework GeO_2 reduction and reoxidation) as very recently reported.[10]

1. Multinuclear NMR

^{13}C and 1H MAS NMR spectra (not shown) demonstrate the organic SDA is occluded intact in the zeolites. The ^{29}Si CP MAS NMR spectra of several relevant germanosilicate HPM-1 samples are shown in Figure 5. The lower trace in the figure is the direct irradiation ^{29}Si MAS NMR spectrum of the pure silica material, which shows two clear resonances at -106.2 and -113.6 ppm, with a relative intensity ratio close to 4:1, assigned to Si in crystallographic sites T_{1-4} and T_5 , respectively.[27] These correspond to sites in and out of D4R, respectively. Interestingly, introduction of Ge causes a new resonance to appear at lower fields (ca. -103.2 ppm for a $Ge_f=0.167$). If Ge shows a preference to occupy sites within D4R units, see below, the new resonance at -103.2 ppm may be ascribed to $\underline{Si}(\text{OSi})_3\text{OGe}$ sites in D4R. Schmidt et al. and Whittleton et al. found a similar downfield shift for $\text{Si}(\text{Si}_3,\text{Ge})$ (-102 ppm and -104 ppm, respectively) compared to $\text{Si}(\text{Si}_4)$ resonances (-108 ppm) in silicogermanate LTA zeolite.[70] On a close inspection, that resonance shows significant intensity almost down to -90 ppm, suggesting the existence of overlapped $\underline{Si}(\text{OSi})_2(\text{OGe})_2$ resonances. For $Ge_f=0.20$ all the resonances experience a small upfield shift (to 103.7, -107.5 and -114.9 ppm, respectively). Upon a further increase in the level of Ge for Si substitution to $Ge_f=0.40$, the lower field signal is the dominant one and clearly consists of several resonances, while the high field side of the spectrum consists of at least three heavily overlapped resonances (-108.4, -111.8 and -114.9 ppm, respectively, suggesting site T_5 , not belonging to D4R, may be now populated by $\underline{Si}(\text{OSi})_2(\text{OGe})_2$, $\underline{Si}(\text{OSi})_3\text{OGe}$ and $\underline{Si}(\text{OSi})_4$, respectively. This is not unexpected if the fraction of Ge in D4R sites is significant. As the Si content decreases further, the spectra becomes much broader, blurry and noisy. We cannot perform a more quantitative analysis of the spectra because the intensities in the CP spectra depend on the proximity to protons and the direct irradiation ^{29}Si MAS NMR spectra require prohibitively long recycle delays to achieve spectra with decent signal to noise ratios (see Figure S7).

More interesting for a better understanding of these materials is the ^{19}F MAS NMR spectroscopy (Figure 6), which is much sensitive to the type of cavity in which fluoride resides and to its kind of interaction with framework atoms. In the case of zeolites containing D4R, fluoride is typically occluded within this small cavity, and its chemical shift depends on the composition of the D4R. The pure silica HPM-1 material displays a single resonance

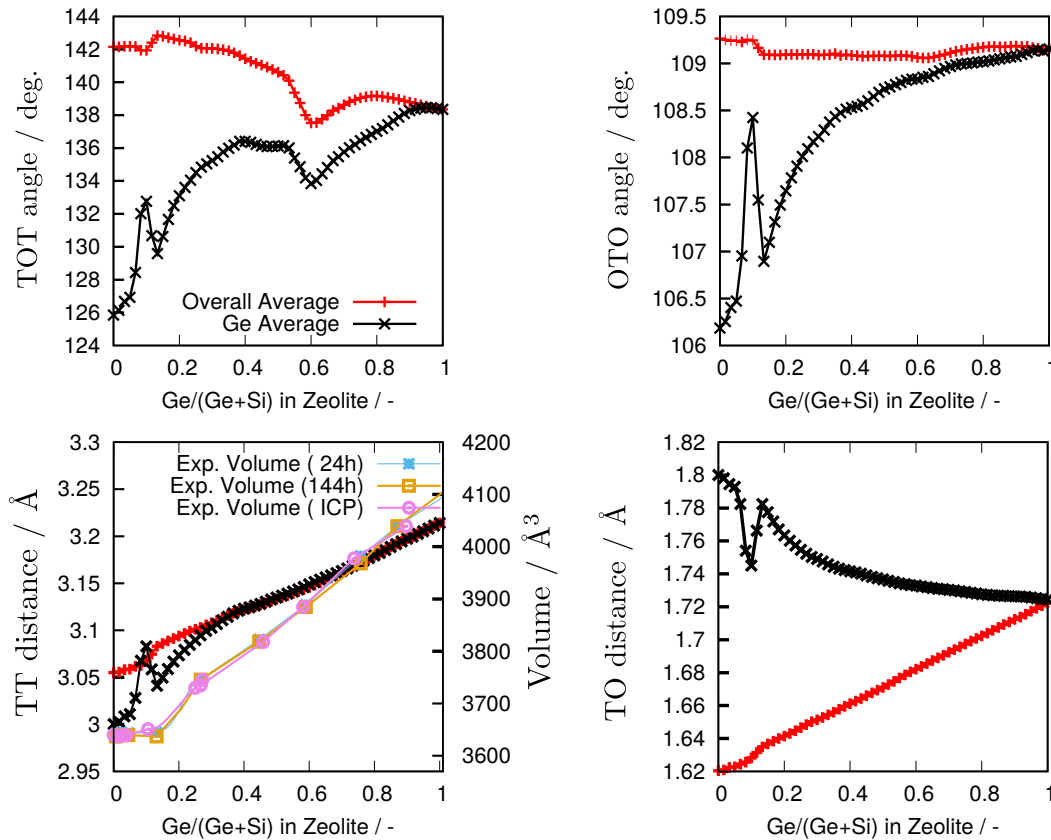


Figure 4. TT averaged distance (Bottom Left), TO average distance (Bottom Right), TOT average angle (Top Left), and OTO average angle (Top Right) versus Ge_f . Red and black points represent the overall average and average which involve tetrahedrons with Ge atoms, respectively.

at around -35.7 ppm, that we will call here resonance 'I'. The assignment of resonance I to F^- occluded in purely siliceous D4R (i.e., 8Si,0Ge D4R) is well established for several pure silica zeolites,[72–75] as well as for pure silica STW,[27] despite the fact that in this zeolite it appears quite downfield shifted compared to more typical values (-37/-40ppm).[74] When Ge is introduced in the synthesis mixture, even in minute amounts ($Ge_f=0.009$), a new resonance appears around -16.6ppm (resonance 'II'). As more Ge is introduced, this resonance first increases, then decreases in intensity, while it experiences an upfield shift (up to -17.5 ppm). Upon increasing the Ge content above $Ge_f = 0.032$ a broad resonance ('III') appears around -7.5 ppm and increases in intensity while shifts to lower field up to $Ge_f=0.4$. We note here that the very significant changes just commented occur in a range of Ge_f in which the zeolite framework appears to be reluctant to expand, as mentioned above (see Figure 3). Then, an apparent upfield shift starts, while the resonance becomes narrower. This apparent change in shift, the narrowing of the band, and prior literature reports on other zeolites lead us think that there is a fourth resonance (IV, around -10/-11 ppm), rather than one that first moves downfield then jumps upfield, and that at intermediate Ge fractions resonances III and IV severely overlap. Since the pure

germanate end-member displays a single, relatively narrow and pretty symmetrical resonance IV at -11.0 ppm, we would initially assign it to F^- occluded in D4R built only of Ge and O (i.e., 0Si,8Ge D4R) (literature values vary roughly in the -9 to -16 ppm).[76]

The assignment of the remaining ^{19}F resonances, II and III, is intriguing and has been the subject of debate. There are typically four types of resonances in the ^{19}F MAS NMR spectra of (Si,Ge)-zeolites containing D4R, despite the fact that, in principle, there may be up to nine different Ge contents in a D4R unit (from 0 to 8) and for several of these contents there may be a number of different configurations of Si and Ge within the D4R, see below. The scarce number of resonances could be just due to resonance overlapping, to some configurations being prohibited or scarce or to an insensitiveness of ^{19}F to certain differences among configurations and compositions. Sastre et al. assigned resonances at -38, -20 and -8ppm in silicogermanates ITQ-17 and ITQ-7 to F^- in nD4R with, respectively, 8, 7, and either 5 or 6 Si atoms, being more favorable to 5.[77, 78] Wang et al. studied octadecasil silicogermanates synthesized with three different SDA cations, covering for two of them the whole range of Ge_f from 0 to 1. The pure silica and pure germania end members present resonances at around -38 and -15 ppm,

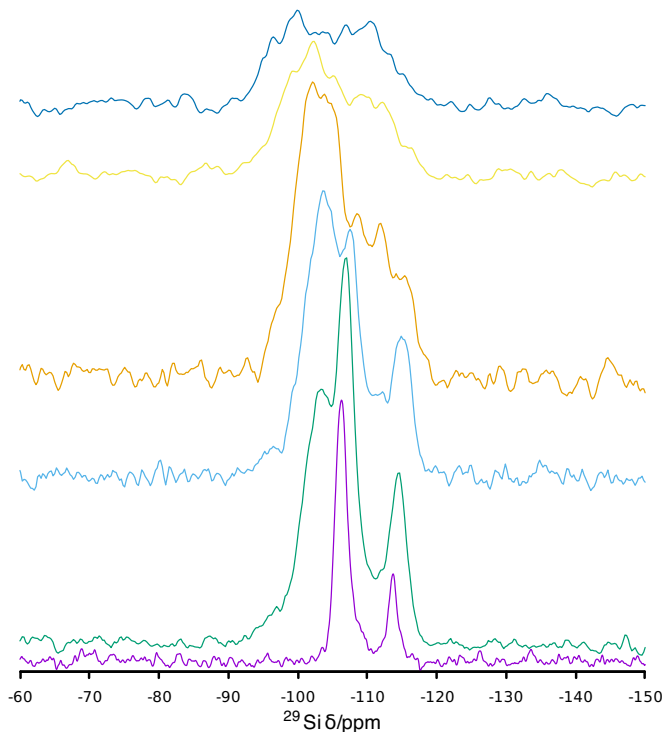


Figure 5. ^{29}Si MAS spectra of (Ge,Si)-STW with $\text{Ge}_f = 0.00, 0.166, 0.20, 0.40, 0.60$ and 0.80 (from bottom to top). The lower trace is a direct irradiation spectrum while the rest were collected under cross polarization.

which are thus assigned to F^- in D4R with 8 and 0 Si, respectively. For intermediate compositions resonances around -8 and -19 ppm were assigned to the presence of 4 and 6 Si per D4R, respectively, and the authors concluded there is an ordered pattern of Ge insertion in the D4R units in which Ge-Ge pairing tend to be avoided.[80] To complicate things, each one of these resonances may change position depending on the Ge_f ,[79] or occluded SDA cation.[81]

Latter on, Sastre et al. suggested that there may exist direct covalent Ge-F bonds in D4R units, with expansion of the coordination of the involved Ge to 5.[82] The same authors calculated the chemical shifts of fluoride occluded in different configurations of D4R units containing 0, 1, 2, 3, 4 or 8 Ge atoms (but they did not consider 5, 6 or 7, for undisclosed reasons) and concluded that, due to the displacement of fluoride out of the cage center and towards a corner, the main factor determining the chemical shift of fluoride was the nature of the 4 closest T, i.e., the n number of closest Si and m number of closest Ge, with $n + m = 4$. [37] Thus, the chemical shift of fluoride increased (values more positive) when the number m of Ge atoms closer to F increased. This could explain that fluoride in D4R containing $4\text{Si}4\text{Ge}$ would resonate at a similar chemical shift as those in $5\text{Si}3\text{Ge}$. This view differs significantly from that of Wang et al. described above,[80] because if Ge-Ge pairings were avoided the

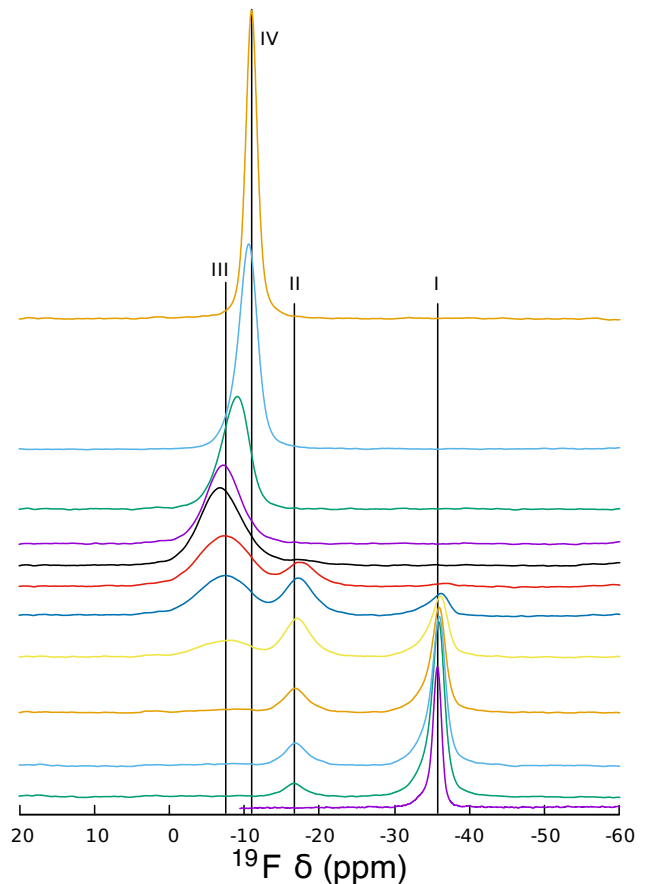


Figure 6. ^{19}F MAS NMR spectra of (Ge,Si)-STW with $\text{Ge}_f = 0.00, 0.009, 0.019, 0.032, 0.09, 0.166, 0.20, 0.40, 0.60$ and $0.80, 0.9$ and 1.00 (from bottom to top). The four types of resonances found are marked with the vertical lines I-IV, placed at the position where they appear at lower Ge_f (except line IV, placed at the resonance of the pure germanate.)

$4\text{Si}4\text{Ge}$ D4R unit would have $m = 1$ Ge as closest neighbours to F.

After deconvolution of the assumed III+IV resonance in the spectra of materials with Ge_f in the 0.6 – 1.0 range, the evolution of the four resonances as a function of the Ge content in the gel is shown in Figure 7, top left, solid lines. It is worth noting that, at the high silica side of the substitutional series, the ^{19}F resonances change very drastically as the Ge_f increases. The sharp decrease of resonance I, which is replaced by resonance II and then III occurs in a range of Ge_f that, as discussed above, shows essentially no variation in unit cell parameters. For a Ge_f of 0.09 the spectrum consists of resonances I, II and III with roughly similar intensities ($\approx 37:38:25$), while the unit cell shows essentially no variation in dimensions.

At first sight, there would be little question about the assignments of resonances I, II and IV. In the case of resonances I and IV the assignment would apparently get strong support from the spectra of the pure SiO_2 and GeO_2 end members, respectively, in which resonances I

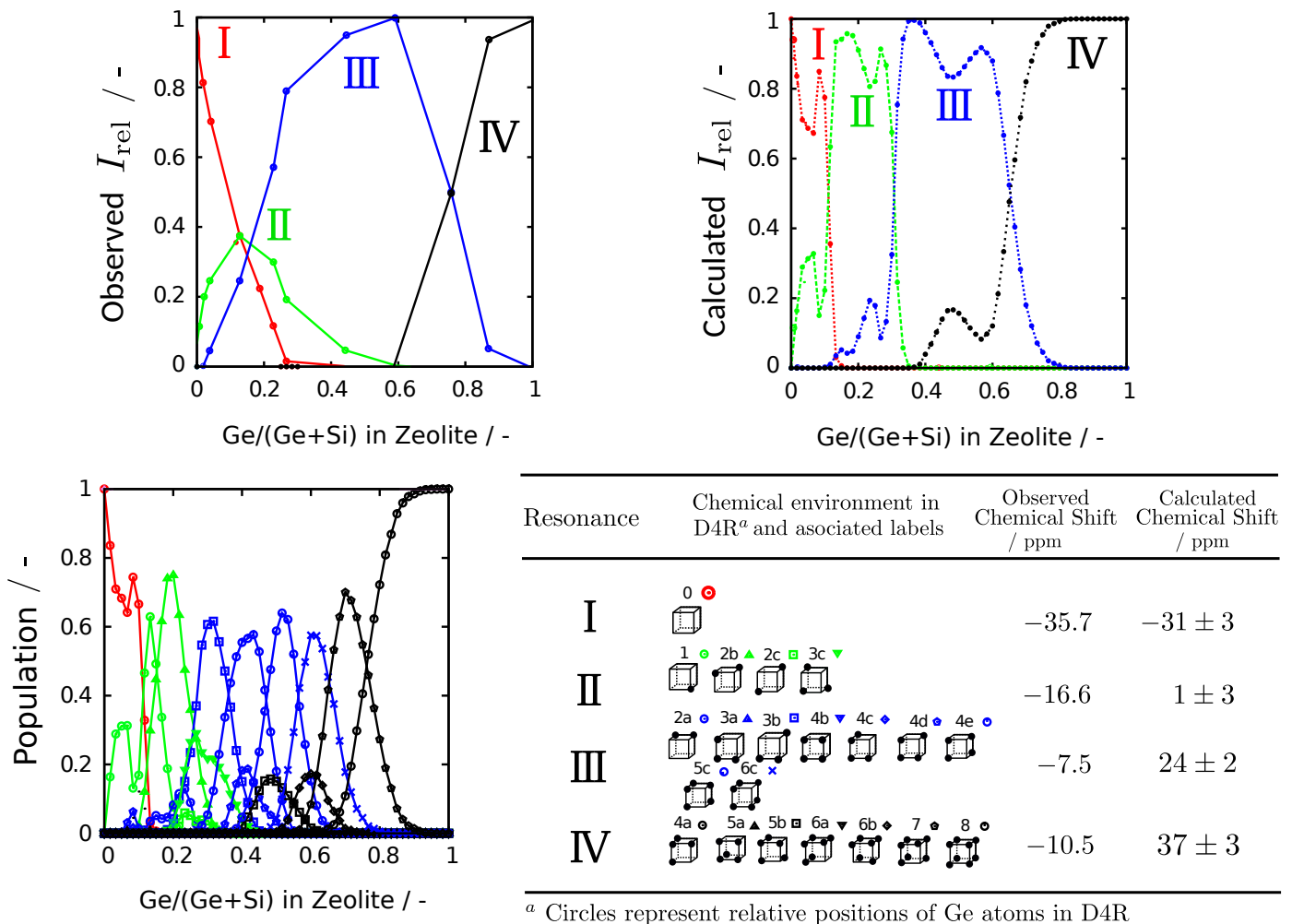


Figure 7. Top: Relative intensities of the four resonances observed in the ^{19}F MAS NMR spectra of (Ge,Si)-STW zeolites as a function of the Ge fraction in the zeolites, Ge_f (left: experimental; right: convolution of calculated populations of chemical environments in D4R, grouped by similar calculated chemical shift). Bottom-Left: Calculated population of chemical environments in D4R as a function of Ge_f . Bottom-Right: Our proposed assignment of observed ^{19}F MAS NMR resonances to chemical environments in D4R, with experimental and averaged calculated chemical shifts.

and IV have no other possible assignment. In the case of II, its appearance at very low Ge_f together with its fast growth and decay as Ge_f increases, would apparently support the assignment to 7Si1Ge-D4R. Resonance III is, obviously, a problem, and the fact that there is only one such resonance implies that either there is a very ordered pattern of Ge introduction (as proposed by Wang et al.)^[80] or at least this resonance actually consists of several resonances overlapped (as suggested by Pulido et al.)^[37]

We made use of DFT calculations in an attempt to shed light on the origin of the four different resonances. It turned out (Figure 7) that the assignments are likely much more complicated than as presumed above or as described in the prior literature. The computed chemical shifts cluster around four well-defined ranges, which can be reasonably well matched to the observed ^{19}F resonances. We have labeled the four set of resonances that

result from the calculations using the same numerals of the analogous experimental resonances, i.e. accordingly to the order the resonances appear in the experiments as the Ge content increases. It is interesting to note that, except resonance I (associated to pure silica units), each resonance has contributions from various configurations, including some with different distributions of Si-Ge atoms in the D4R units (Figure 7, bottom-right). Based on the dispersion of the computed values of the chemical shifts, we assign the observed four resonances to F atoms occluded in D4R cages with the following Ge content and Ge clustering pattern:

1. no Ge atoms (resonance I)
2. isolated Ge atoms, i.e. Ge atoms with three Si atoms as cage neighbours (resonance II). Thus, there may be 1-3 Ge atoms in the D4R.
3. Ge pairs not satisfying the conditions of type IV

(resonance III). Here, up to nine different configurations with 2-6 Ge atoms are possible.

4. closed Ge clusters, i.t. configurations with at least one Ge possessing three Ge atoms as next nearest neighbours (resonance IV). There may be seven different such configurations with 4-8 Ge atoms.

The proposed assignment is not simply based on the number of Ge atoms in the D4R unit, but mainly on how Ge atoms are distributed in that unit with regard to F, so that the very local chemical environment of the F atoms is constant within each group responsible for the four resonances. For example, the F atoms in D4R configurations *1* and *2b* (Figure 7, bottom left) have similar chemical environments, since the core electrons of the F atom in configuration *2b* are being affected mainly by just one Ge atom, as if it were in a 1 Ge-containing D4R. Accordingly, in configuration *2a*, in which the two Ge atoms are nearest neighbors, the core electrons of the F atom sense the simultaneous presence of two Ge atoms. As we have noted in the methodology, the covalency of the F environments in the D4R is expected to affect the NMR calculation. The deviation of the predictions with respect to the experimental values increase with the number of Ge presents in the nearest environment of fluoride atoms in the D4R, i.e. the covalency, maintaining the statistical error of the calculations constant. The deviation is proportional to the numeral of the resonance, and it is about a constant value of 15 ppm (see Figure S8). Note that the apparent uncorrelated calculation of the chemical shift of such large system using the PBE functional acquire rationalization through this analysis and provides a means to understand and predict chemical shifts of F in those structures.

It is worth noting that the presence of resonance III at the high silica side of the substitutional series (very dimly at $Ge_f=0.032$ but robustly evident at $Ge_f=0.09$) implies significant formation of Ge-O-Ge bonds at relatively low Ge contents, according to our assignment. We find this, however, rather logical because, as we will see below, sites T1 and T2 are clearly the preferred sites to be occupied by Ge and they are multiply connected to each other (each T1 or T2 connects to one T1 and one T2). Then, Ge-O-Ge formation at low Ge_f suggests that there must be no significant penalty for Ge pairing in zeolites, as opposed to prior suggestions of a Ge-Ge avoidance at $Ge_f < 0.5$. [80]

Supported by the good agreement observed between the synthesis yield and the computed free energy of the solids, we use these energy values to construct the set of representative Ge configurations for each Ge content, covering the whole Ge-containing compositional range, i.e. from 1 to 60 Ge atoms per unit cell. We considered the configurations whose sum of occurrences of probability are at least 99.9 %. Taking into account the assignment of the DFT-computed NMR resonances, as well as the chemical environments identified, we recreated the theoretical population of the F-NMR resonances. The

comparison between theoretical resonances and experimental intensities of the observed resonances is qualitatively good, as can be observed in Figure 7, top left, dotted lines, which suggests that the distribution of chemical environments is reasonably well represented in the space of possible configurations that the effective Hamiltonian predicts (Figure 7, top right). In this respect, differences between theoretical and experimental findings may be due to heterogeneity in the composition of the D4R. For example, for $Ge_f = 0.5$ a small contribution for resonance IV appears in the calculated population curve (Figure 7-top right) that is absent in the experimental spectrum. Note that this calculated intensity for the resonance IV is again retrieved for $Ge_f = 0.65$, which supports the view of heterogeneity in the composition as the main source of the observed small differences. Inaccuracies of the used interatomic potential, not being fine enough to see the small variations in Si-Ge distribution within the D4R units might be also a source for the mismatch.

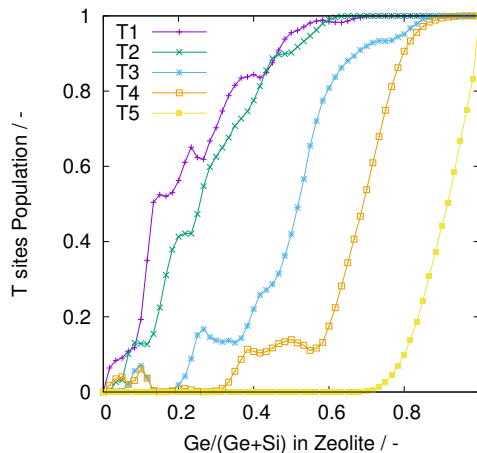


Figure 8. Variation of the populations of the different T sites, as a function of Ge content in zeolite, Ge_f , calculated with the EH.

We can also get an insight into the different preference of Ge (Si) to occupy the different crystallographic T-sites. Employing an effective Hamiltonian, we obtained the population of each T site as a function of the Ge_f , as shown in Figure 8. According to these calculations, the Ge preferential occupation of sites goes in the order $T1 \geq T2 > T3 > T4 > T5$. Thus, as the Ge content increases, sites T1 and T2 are occupied first. Then site T3 followed by T4 start to be occupied at relatively low Ge contents but with a lower preference over T1 and T2. Finally, after sites T1 and T2 are fully occupied but before the rest of sites in the D4R units are occupied, site T5 begins to be occupied by Ge atoms.

In the following section we shall compare the preferential occupation of the different sites predicted by molecular simulations with that obtained from Rietveld analysis.

2. Rietveld refinement

In order to get a deeper experimental insight into the Ge-Si substitution in HPM-1, we performed Rietveld refinements of the structures of samples prepared at $Ge_f = 0.4$, 0.6 and 1.0 using powder data collected using synchrotron radiation, and the details are given in the Supporting Information.

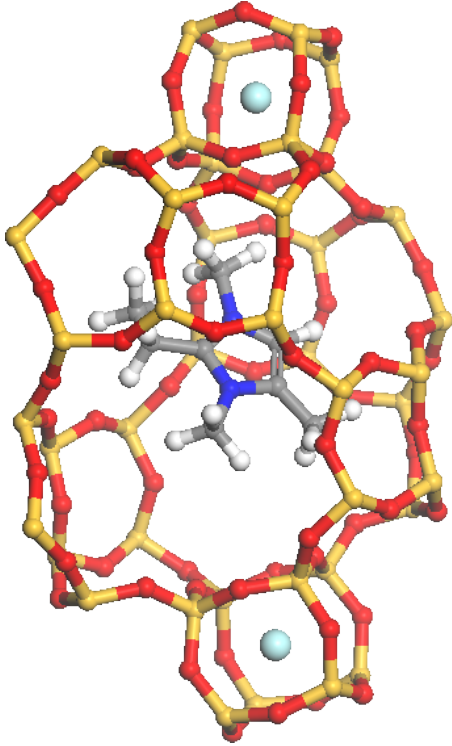


Figure 9. The organic SDA cation inside the large $[4^6 5^8 8^2 10^2]$ cage (only one of the two symmetrical cations is shown) and the fluoride anion inside the small $[4^6]$ cage of Ge-HPM-1.

The final refined structures have reasonable unrestrained bond distances and angles (see Table S3) and all show the fluoride anions slightly off the center of the D4R cages and closer to T1 than to any other tetrahedral atom in the framework. Figure 9 shows the organic cation and fluoride anions occluded in their respective cages in the purely GeO_2 HPM-1. The refined occupancies of Ge and Si in the $Ge_f = 0.4$ and 0.6 samples are close to the nominal values (0.40 and 0.57, respectively) and both show a distinct preference for Si rather than Ge to occupy T5 (the non-D4R site) and a Ge preference to occupy sites T1 and T2 over T3 and T4 (see Table I). The site occupancies observed in these samples roughly agree with the order of preferential occupations determined from our calculations (see Figure 8). In both cases, as the amount of Ge increases, T1 and T2 are populated before T3 and T4, which in turn get occupied preferentially over T5. There are, however, quantitative discrepancies between both results. The first one is that the differences in occupation between sites T1 and T2 and between sites T3

and T4 are larger in our calculations than in the experiments. And the second discrepancy is that experimentally T5 starts being slightly populated at $Ge_f = 0.4$, and at $Ge_f = 0.6$ its population is already roughly one third of either one of T3 and T4, while at that point T1 and T2 are not fully occupied by Ge yet. This is in clear contrast with the predicted values, which show that T5 does not start being populated by Ge until all other sites are filled, or almost filled. Roughly speaking, our calculations predict more strict preferential occupations and, hence, more abrupt changes in population trends. There are mainly two possible explanations for these discrepancies. First, we could ascribe the differences to inaccuracies of the energy calculation employed, which might be making T5 sites too unstable for Ge compared with the other sites. While this might be the case, it is also possible that we are neglecting some factors in our calculations. Namely, our calculations are based on the analysis of the thermodynamic properties of the system in equilibrium. But it is well known that kinetic factors play a relevant role in the formation of zeolites, i.e. the system might have a mixture of metastable configurations, and configurations that appear purely for kinetic reasons, and we are missing all of those in our analysis. These kinetic factors would smooth the tendencies observed in the calculations. But apart from these discrepancies, both sets of data provide the same general view, consisting in the similar Ge population of sites T1 and T2, followed by T3 and T4, and finally T5.

Table I. Refined Ge occupancies of T sites in Ge,Si-HPM-1

| | Overall $Ge_f = 0.4$ | Overall $Ge_f = 0.6$ |
|----------|----------------------|----------------------|
| Ge in T1 | 0.552 | 0.748 |
| Ge in T2 | 0.555 | 0.735 |
| Ge in T3 | 0.388 | 0.584 |
| Ge in T4 | 0.393 | 0.591 |
| Ge in T5 | 0.092 | 0.215 |

IV. CONCLUSIONS

Isomorphous substitution of Si by Ge in the synthesis of zeolite STW using 2-ethyl-1,3,4-trimethylimidazolium and fluoride affords the crystallization of the whole substitutional series from the pure SiO_2 to the pure GeO_2 end-members. A combined experimental-theoretical approach allowed us to get significant insight into the system, which may be of general interest for germanosilicate zeolites. As the Ge molar fraction increases, the yield of zeolite goes through a maximum and then severely drops at the GeO_2 end member. Our calculation of the corresponding free energies matches well the inverse of the yield curve.

The isomorphous substitution of Si by Ge brings about an expansion of the structure that is roughly linear for most of the series. However, for low Ge_f (≤ 0.1) there is no expansion of the unit cell. This resilience to expansion

is attributed to the local deformability around Ge atoms and the higher rigidity of SiO_2 .

Similarly to previously published germanosilicate zeolites containing double 4-ring units (D4R), we observe up to four distinct resonances in the ^{19}F MAS NMR spectra, depending on the Ge content. However, the assignment of these resonances is far more complicated than previously thought. Density functional theory calculations of the ^{19}F chemical shifts of fluoride occluded in every possible configuration of every $[\text{Si}_{(8-n)}\text{Ge}_n]$ D4R unit (with $0 \leq n \leq 8$) reveals the resonances are not simply dependent on the number n of Ge atoms but also on the extension of Ge pairing. Thus, resonances are assigned to fluoride occluded in D4R with no Ge, with isolated Ge, with Ge pairs or with Ge in closed clusters.

Our modelling of these materials showed the presence of a complex energy surface with multiple shallow minima. We suggest that even static modelling of materials may thus provide means for predicting their flexibility.

Finally, we studied the preferential occupation of crystallographic sites by Ge both theoretically (for the whole series) and experimentally (by Rietveld refinement of structures with different Ge_f using synchrotron powder diffraction data). We found a good overall agreement but with a somewhat more abrupt and sharply distinct preferences in the models than in the experimental results. This is attributed to both the limitations of the theoretical approach and to kinetic factors allowing the real existence of metastable configurations not considered by the models.

V. CONFLICTS OF INTEREST

There are no conflicts to declare.

ACKNOWLEDGEMENTS

The authors thank the Spanish Ministry of Science and Competitiveness for funding (Projects MAT2015-71117-R and CTP2016-80206-P). R.T. Rigo thanks CAPES (Brazil) for a PhD fellowship (process 99999.012012/2013-00). S.R.G. Balestra thanks the Spanish State Secretariat for Research, Development and Innovation for his predoctoral fellowship (BES-2014-067825 from CTQ2013-48396-P). We are also indebted to the ERSF (Grenoble) and the BM25 Spline staff, particularly to G. Castro and A. Serrano as well as to L. A. Vilaescusa (Valencia) for help in collecting the synchrotron XRD data and for helpful comments and suggestions. We also thank A. Valera for technical expertise (FESEM). Computing facilities by Alhambra supercomputing center (Universidad de Granada) is grateful acknowledge.

Appendix A: Supplementary Information available

Ge_f in zeolites as a function of Ge_f in gel, Calculation of the energy of the configurations, synthesis results, cell parameters vs Ge_f computed with Effective Hamiltonians, some of the energy-minimised D4Rs configurations, infrared spectra, FE-SEM images, thermograms, direct irradiation ^{29}Si MAS NMR, difference between calculated and experimental ^{19}F chemical shifts, Rietveld details, Rietveld plots, Table of crystallographic and experimental parameters, average bond distances and angles (Tables S1-S4 and Figures S1-S11).

1. Methodology

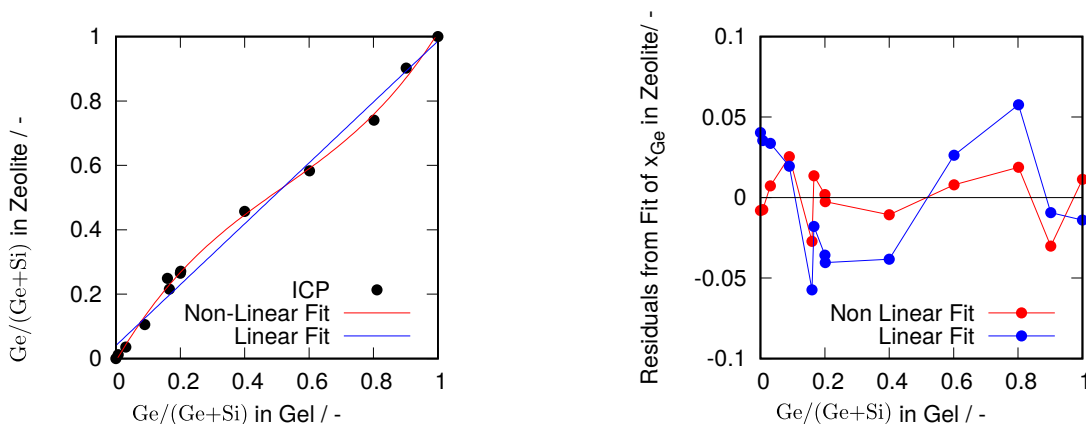


Figure S1. Molar fraction of Ge in the zeolites as a function of that in the gel.

Table S1. Details of the number of configurations used for each Ge content

| Ge/Si | Total number of configurations | Number of inequivalent configurations |
|-------|--------------------------------|---------------------------------------|
| 1 | 60 | 5 |
| 2 | 1770 | 165 |
| 3 | 34220 | 2855 |
| 4 | 487635 | 40890/ 1507 ^a |

^a The number of configurations considered in the calculations is shown in bold type.

a. Calculation of the energy of the configurations: Effective Hamiltonian approach

The incorporation of heteroatoms in a zeolite framework might generate a large configurational space of possible atomic distribution. For simplicity, we will concern only on binary composition, for instance in the case of the present case Si-Ge distribution. Symmetry consideration, by using the SOD program,[34] allows us to map all non-equivalent configurations up to 4 Ge atoms by unit cell. Since the cell contains 60 tetrahedral sites and the symmetry of the pure silica STW zeolite framework is relatively low (space group # 178), with 4 Ge atoms by unit cell there are already more than 40 thousand configurations. Even by using interatomic potential based calculations, this is already a heavy computational effort. For larger increase of the minority element in the binary solid solution, the number of configurations increases exponentially and therefore it is not possible to compute their energy. To deal with this, we turn to the recently developed Effective Hamiltonian (EH) approach [32], which parametrise the atom-atom interaction in a simple numerical function. In this way, the energy of millions of configurations can be evaluated at a small computational cost. Nevertheless, the method implies an initial high cost, since all configurations having 2 Ge (for STW a total of 165) and 3 Ge (2855 configurations) are needed first to submit to full energy relaxation, including atomic coordinates and cell parameters. Since Ge atoms confers large structural flexibility to the framework, those configurations having 4 Ge atoms, with either 4 nearest Ge neighbours or 3 Ge neighbours plus a 4th Ge atom as

second next nearest neighbour, were also considered for the parameterisation of the EH. The set of zeolites considered with 4 Ge atoms has 1507 configurations.

The EH is based on consideration that the entrance of a heteroatom can be treated as a defect. First the substitution energies for isolated Ge atoms in the five distinct T sites are computed and after that, the interaction energies with the addition of new Ge atoms are computed. We therefore parameterise the effective Hamiltonian as follows:

1. Firstly, the perturbation energy to substitute a Ge atom, $\Delta E(\vec{r}_i)$, is calculated using the Mott-Littleton methodology [33], for each unique tetrahedral site \vec{r}_i .

$$\Delta E(\vec{r}_i) = E_i - E_0 \quad (\text{S1})$$

where E_0 and E_i are the lattice energies computed with GULP using the interatomic potential of pure silica structures and structures with one Ge/Si substitutions.

2. We then consider a pair interaction energy denoted as $\Delta E(\vec{r}_i, \vec{r}_j)$, where \vec{r}_i and \vec{r}_j are two tetrahedral sites, and is computed as the difference in energy between the individual energies for placing Ge atoms at sites i and j (i.e. $\Delta E(\vec{r}_i)$ and $\Delta E(\vec{r}_j)$ from above) and the energy found when both sites are occupied in a periodic calculation. The perturbation energy is given by:

$$\Delta E(\vec{r}_i, \vec{r}_j) = E_{ij} - \Delta E(\vec{r}_i) - \Delta E(\vec{r}_j) - E_0 \quad (\text{S2})$$

where E_{ij} is the lattice energy of structures with two Ge/Si substitutions.

3. Idem for trios and quartets of atoms.

$$\begin{aligned} \Delta E(\vec{r}_i, \vec{r}_j, \vec{r}_k) &= E_{ijk} - \Delta E(\vec{r}_i, \vec{r}_j) - \Delta E(\vec{r}_i, \vec{r}_k) - \Delta E(\vec{r}_j, \vec{r}_k) - \\ &\quad - \Delta E(\vec{r}_i) - \Delta E(\vec{r}_j) - \Delta E(\vec{r}_k) - E_0 \end{aligned} \quad (\text{S3})$$

$$\begin{aligned} \Delta E(\vec{r}_i, \vec{r}_j, \vec{r}_k, \vec{r}_l) &= E_{ijkl} - \Delta E(\vec{r}_i, \vec{r}_j, \vec{r}_k) - \{\dots\}^{ijk} - \Delta E(\vec{r}_j, \vec{r}_k, \vec{r}_l) - \\ &\quad - \Delta E(\vec{r}_i, \vec{r}_j) - \{\dots\}^{ijkl} - \Delta E(\vec{r}_k, \vec{r}_l) - \\ &\quad - \Delta E(\vec{r}_i) - \Delta E(\vec{r}_j) - \Delta E(\vec{r}_k) - \Delta E(\vec{r}_l) - E_0 \end{aligned} \quad (\text{S4})$$

where $\{\dots\}^{ijk}$ and $\{\dots\}^{ijkl}$ represent all the summation terms, which are combinations of the ijk and $ijkl$ indices, respectively.

Then, an effective approximate lattice energy of N Si/Ge substitutions is being calculated as:

$$\begin{aligned} \mathcal{H} &= E_0 + \sum_i \Delta E(\vec{r}_i) + \sum_{ij} \Delta E(\vec{r}_i, \vec{r}_j) + \sum_{ijk} \Delta E(\vec{r}_i, \vec{r}_j, \vec{r}_k) + \\ &\quad + \sum_{ijkl} \Delta E(\vec{r}_i, \vec{r}_j, \vec{r}_k, \vec{r}_l) + \mathcal{O}(\vec{r}^{2N}) \end{aligned} \quad (\text{S5})$$

where i, j, k, l -indexes run on the total number of configurations. Is useful to adapt the Equation S5 with a *tensor* notation using the Einstein summation convention:

$$\mathcal{H}(N) = E_0 + \epsilon_i S^i + \rho_{ij} S^i S^j + \theta_{ijk} S^i S^j S^k + \phi_{ijkl} S^i S^j S^k S^l \quad (\text{S6})$$

where S^i are spin-type variables with 1 or 0 represent the presence or absence, respectively, of Ge atom in the crystallographic i -position, $\epsilon := \{\Delta E(\vec{r}_i)\}$, $\rho := \{\Delta E(\vec{r}_i, \vec{r}_j)\}$, $\theta := \{\Delta E(\vec{r}_i, \vec{r}_j, \vec{r}_k)\}$ and $\phi := \{\Delta E(\vec{r}_i, \vec{r}_j, \vec{r}_k, \vec{r}_l)\}$. We can readapt the Equation S6 to sum on the inequivalent configurations using a dictionary, δ , which connects each configuration with the calculated equivalent configuration.

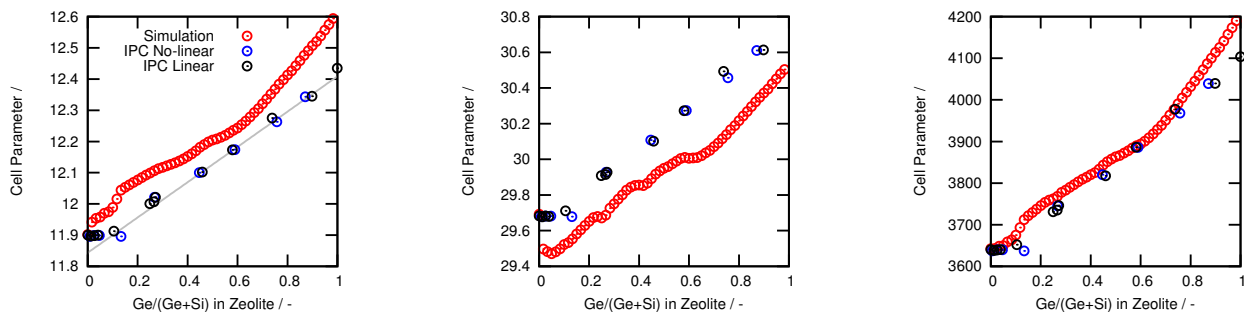
$$\begin{aligned} \mathcal{H}(N) &= E_0 + \epsilon_\alpha \delta_i^\alpha S^i + \frac{\rho_{\alpha\beta}}{N-1} \delta_{ij}^{\alpha\beta} S^i S^j + \frac{2\theta_{\alpha\beta\gamma}}{(N-2)(N-3)} \delta_{ijk}^{\alpha\beta\gamma} S^i S^j S^k + \\ &\quad + \frac{2\phi_{\alpha\beta\gamma\zeta}}{(N-3)(N-4)} \delta_{ijkl}^{\alpha\beta\gamma\zeta} S^i S^j S^k S^l \end{aligned} \quad (\text{S7})$$

2. Results

Table S2. Summary of synthesis results at 175 °C

| Ge_f | Time (hours) | Yield (wt. %) | Phase ^a |
|--------|--------------|---------------|-----------------------------|
| 0 | 27 | 31.1 | amorphous (+ HPM-1) |
| 0 | 48 | 21.2 | HPM-1 |
| 0 | 143 | 29.7 | HPM-1 |
| 0 | 264 | 29.6 | HPM-1 |
| 0.009 | 25 | 22.5 | HPM-1 + amorphous |
| 0.009 | 48 | 23.7 | HPM-1 |
| 0.009 | 144 | 23.7 | HPM-1 |
| 0.009 | 240 | 24.1 | HPM-1 |
| 0.019 | 25 | 25.1 | HPM-1 |
| 0.019 | 48 | 24.1 | HPM-1 |
| 0.019 | 144 | 25.4 | HPM-1 |
| 0.019 | 240 | 25.4 | HPM-1 |
| 0.032 | 25 | 27.1 | HPM-1 |
| 0.032 | 48 | 27.9 | HPM-1 |
| 0.032 | 144 | 26.16 | HPM-1 |
| 0.032 | 240 | 26.3 | HPM-1 |
| 0.09 | 25 | 33.1 | HPM-1 |
| 0.09 | 48 | 31.4 | HPM-1 |
| 0.09 | 144 | 32.2 | HPM-1 |
| 0.09 | 240 | 34.4 | HPM-1 |
| 0.166 | 25 | 34.4 | HPM-1 |
| 0.166 | 48 | 34.5 | HPM-1 |
| 0.166 | 144 | 33.3 | HPM-1 |
| 0.166 | 237 | 36.1 | HPM-1 |
| 0.2 | 25 | 36.4 | HPM-1 |
| 0.2 | 48 | 35.7 | HPM-1 |
| 0.2 | 144 | 36.1 | HPM-1 |
| 0.2 | 240 | 35.5 | HPM-1 |
| 0.4 | 25 | 39.3 | HPM-1 |
| 0.4 | 48 | 39.7 | HPM-1 |
| 0.4 | 144 | 38.0 | HPM-1 |
| 0.4 | 240 | 37.9 | HPM-1 |
| 0.6 | 25 | 24.9 | HPM-1 |
| 0.6 | 48 | 26.8 | HPM-1 |
| 0.6 | 144 | 27.6 | HPM-1 |
| 0.6 | 240 | 32.5 | HPM-1 |
| 0.8 | 25 | 25.4 | HPM-1 |
| 0.8 | 48 | 23.3 | HPM-1 |
| 0.8 | 144 | 26.6 | HPM-1 |
| 0.9 | 25 | 5.5 | HPM-1 |
| 0.9 | 48 | 18.1 | HPM-1 |
| 0.9 | 144 | 21.8 | HPM-1 |
| 1 | 27 | 0 | - ^b |
| 1 | 113 | 1.7 | HPM-1 |
| 1 | 200 | 2.6 | Q+Arg (+HPM-1) ^c |
| 1 | 96 | 10.4 | HPM-1 (+Q) ^{c,d} |
| 1 | 102 | 9.5 | HPM-1 +Q ^{c,d} |

^a Major phases are listed first, very minor phases appear between parentheses. ^b No solids could be collected. ^c Q is the Quartz-like and Arg is the Argutite-like GeO_2 phases. ^d The last two entries correspond to a different synthesis run in the same nominal conditions as the preceding ones.

Figure S2. Cell parameters vs Ge_f computed with the EH.

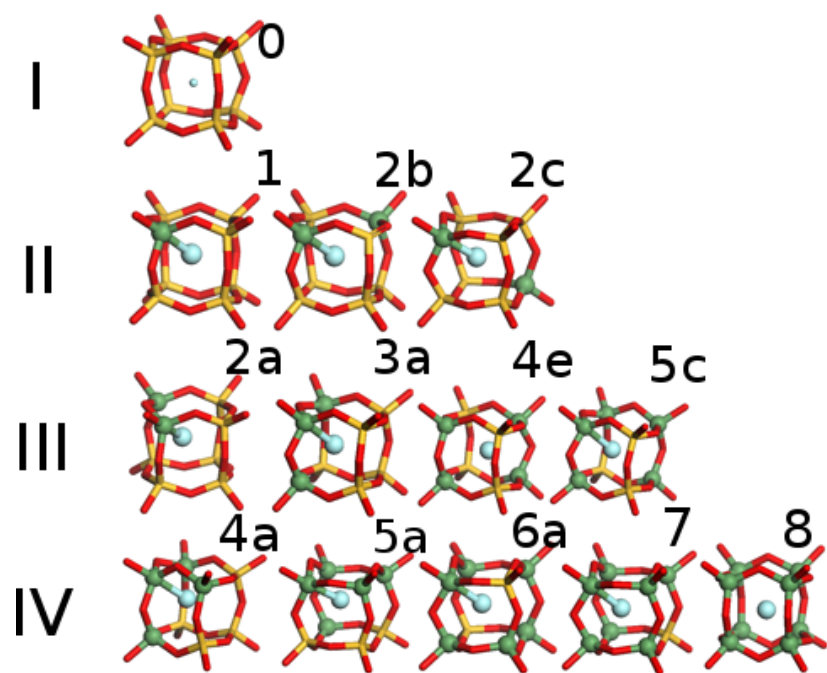


Figure S3. Some of the energy-minimised D4Rs configurations. They are classified according to the resonance. Some structural distortions are distinguishable with respect to the configuration of pure silica.

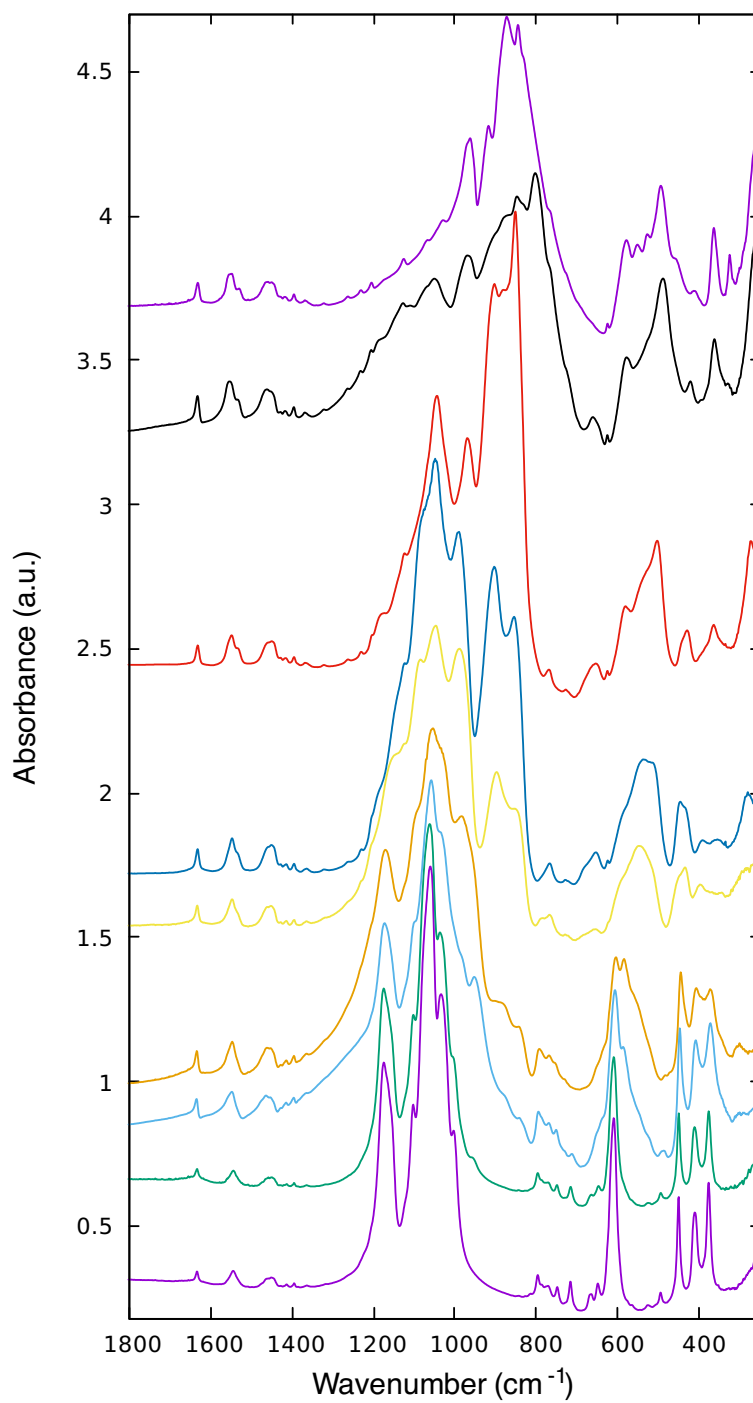


Figure S4. Infrared spectra of STW zeolites obtained from gels with $\text{Ge}_f = 0, 0.01, 0.09, 0.17, 0.4, 0.6, 0.8, 0.9$ and 1 (from bottom to top)

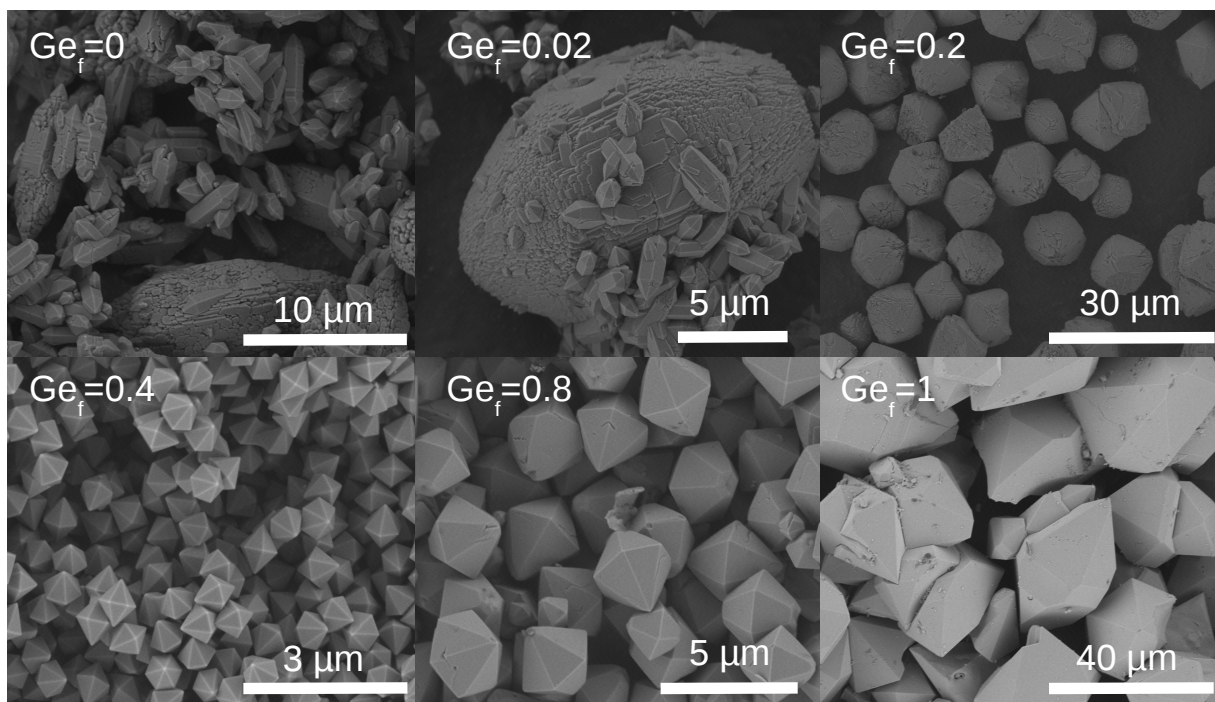


Figure S5. FESEM images of HPM-1 zeolites prepared at different Ge_f levels.

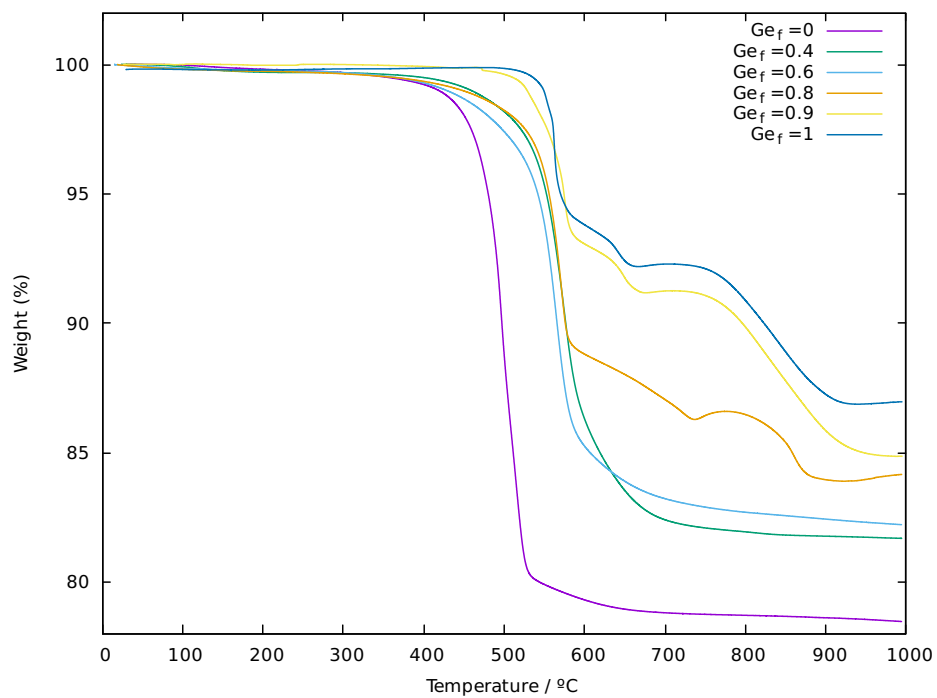


Figure S6. Thermograms of HPM-1 zeolites prepared at different Ge_f levels.

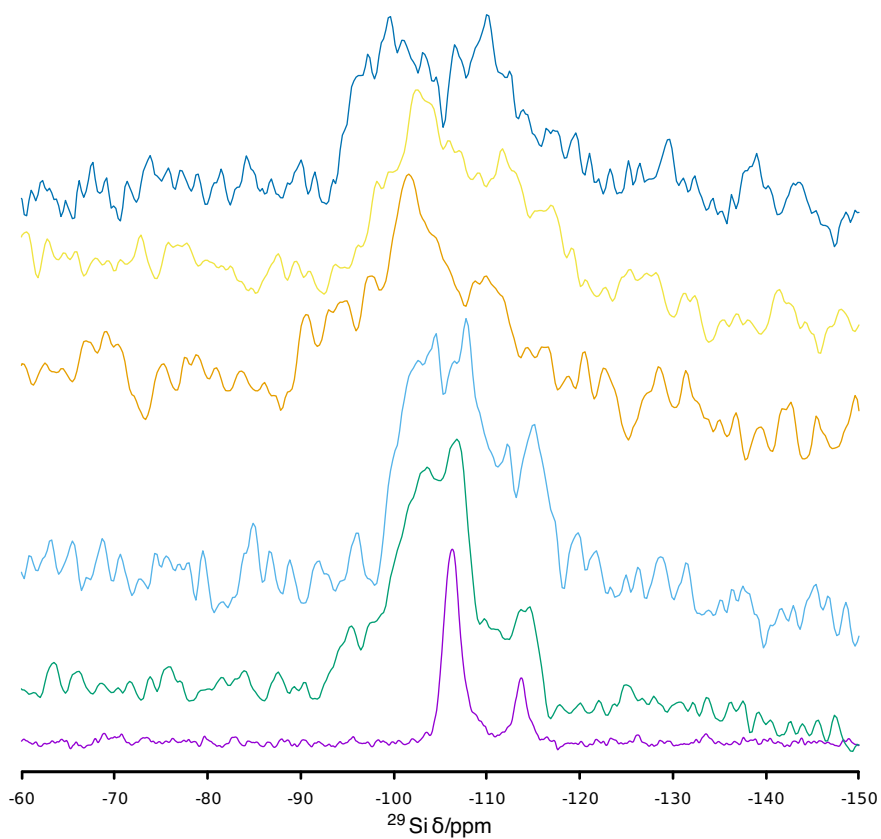


Figure S7. Direct irradiation ^{29}Si MAS spectra of (Ge,Si)-STW with $\text{Ge}_f = 0.00, 0.166, 0.20, 0.40, 0.60$ and 0.80 (from bottom to top). For every spectra 2048 scans were acquired. Recycle delays are 60s for the pure silica sample and 180s for the rest.

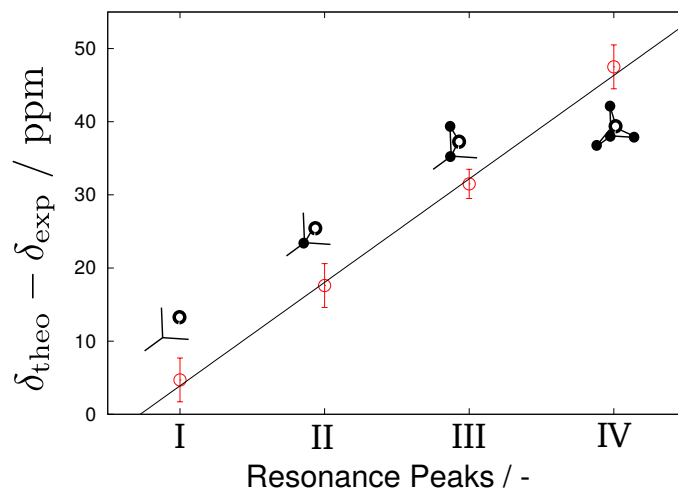


Figure S8. Difference between calculated and experimental chemical shifts for each ^{19}F resonance according to our assignment (see main text).

3. Rietveld details

The starting model for Rietveld refinement of samples prepared with $Ge_f=0.4, 0.6$ and 1 was the refined structure of pure silica HPM-1,[27] in space group $P6_122$ modified to have the unit cell dimensions determined from conventional powder XRD data and a Ge occupation of all crystallographic positions initially set at 0.4, 0.6 and 1.0, respectively (Si occupancies of 0.6, 0.4 and 0.0, respectively). Although the sample with $Ge_f = 1$ appeared as phase-pure in the conventional XRD pattern, synchrotron radiation showed the presence of small traces of quartz-like GeO_2 , and the corresponding regions were excluded from the refinement. A Lobanov and Alte da Veiga absorption correction was applied.[29] Scale factor, unit cell and profile parameters were refined, with a shifted Chebyshev function initially with 16 fixed parameters to simulate the background. Then, the Ge, Si, O and F atoms were allowed to move, initially with soft restrains on T-O and O-O distances and with Ge and Si in each crystallographic site constrained to move together. Then, the position and orientation of the organic SDA was refined as a rigid body consisting of the imidazolium ring with the three methyl substituents as a rigid unit plus the ethyl group as a satellite that could freely rotate along the C2-C9 bond. The hydrogen atoms were omitted but the fractional occupancies of the C atoms were adjusted to account for the electrons of the bonded H. The weight of the distance restrains was gradually reduced and eventually eliminated. In the final stages of the refinements, atom displacement factors (grouped by atom type), background and fractional occupancies of Ge and Si in each crystallographic site (constrained to amount to a full occupancy of each site) were included in the refinement. Final crystallographic data are summarized in Tables S3, the final Rietveld plots are given in Figures S9, S10 and S11 and the corresponding cif files are provided as supplementary material.

Table S3. Crystallographic and Experimental Parameters for the Rietveld Refinement of as-made Ge,Si-HPM-1 phases (wavelength: 0.56383 Å, Temperature 293K)

| | | | |
|-------------------------------|--------------|--------------|--------------|
| Nominal Ge_f | 0.4 | 0.6 | 1 |
| Refined Ge_f | 0.396 | 0.574 | - |
| 2θ range | 2.00-38.32 | 2.00-33.97 | 2.50-44.9 |
| no. of data points | 3733 | 3198 | 4241 |
| no. of reflections | 1327 | 977 | 1792 |
| Space Group | $P6_122$ | $P6_122$ | $P6_122$ |
| unit cell parameters (Å) | | | |
| a, b | 12.09289(16) | 12.16714(17) | 12.42671(11) |
| c | 30.0839(5) | 30.2519(6) | 30.6310(5) |
| Cell volume (Å ³) | 3810.01(12) | 3878.46(13) | 4096.41(8) |
| Residuals | | | |
| R_{wp} | 3.06% | 2.82% | 3.66% |
| R_p | 2.36% | 2.23% | 2.65% |
| R_{F^2} | 7.76% | 7.53% | 10.58% |
| reduced χ^2 | 2.513 | 2.527 | 3.98 |

Table S4. Average bond distances and angles in Ge,Si-HPM-1 phases

| Average distance (Å) | $Ge_f = 0.4$ | $Ge_f = 0.6$ | $Ge_f = 1$ |
|----------------------|--------------|--------------|------------|
| T1-O | 1.654 | 1.662 | 1.668 |
| T2-O | 1.656 | 1.670 | 1.714 |
| T3-O | 1.637 | 1.647 | 1.706 |
| T4-O | 1.667 | 1.689 | 1.724 |
| T5-O | 1.635 | 1.642 | 1.724 |
| T1-F | 2.57 | 2.63 | 2.57 |
| T2-F | 2.79 | 2.76 | 2.89 |
| T3-F | 2.70 | 2.71 | 2.72 |
| T4-F | 2.74 | 2.75 | 2.75 |
| Average angle (°) | | | |
| O-T1-O | 109.3 | 109.2 | 109.2 |
| O-T2-O | 109.4 | 109.4 | 109.3 |
| O-T3-O | 109.1 | 109.0 | 109.4 |
| O-T4-O | 109.4 | 109.4 | 109.2 |
| O-T5-O | 109.4 | 109.4 | 109.6 |

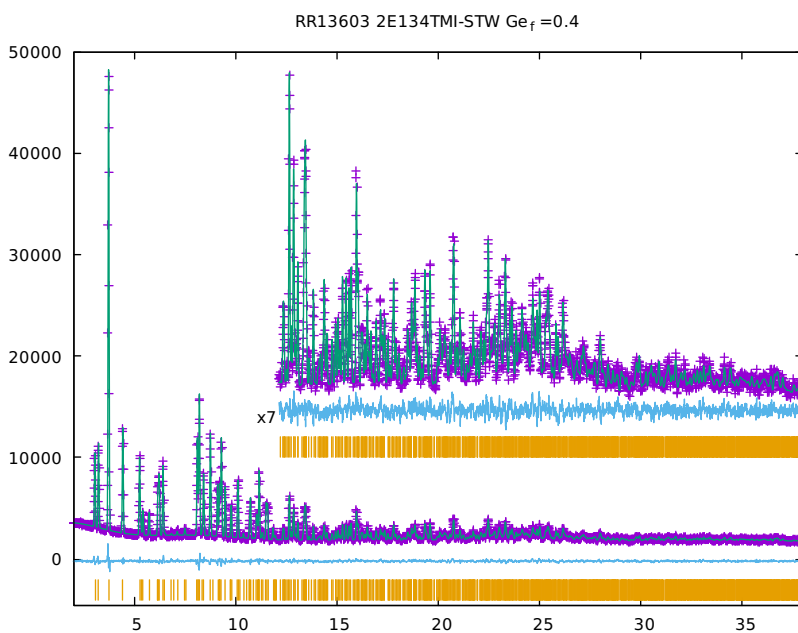


Figure S9. Observed (+) and calculated (solid line) powder X-ray diffractograms for as-made Ge_fSi_{1-f}HPM-1 with $Ge_f = 0.4$ refined in space group $P6_122$. Vertical tic marks indicate the positions of allowed reflections. The lower trace is the difference plot. $\lambda = 0.56383 \text{ \AA}$.

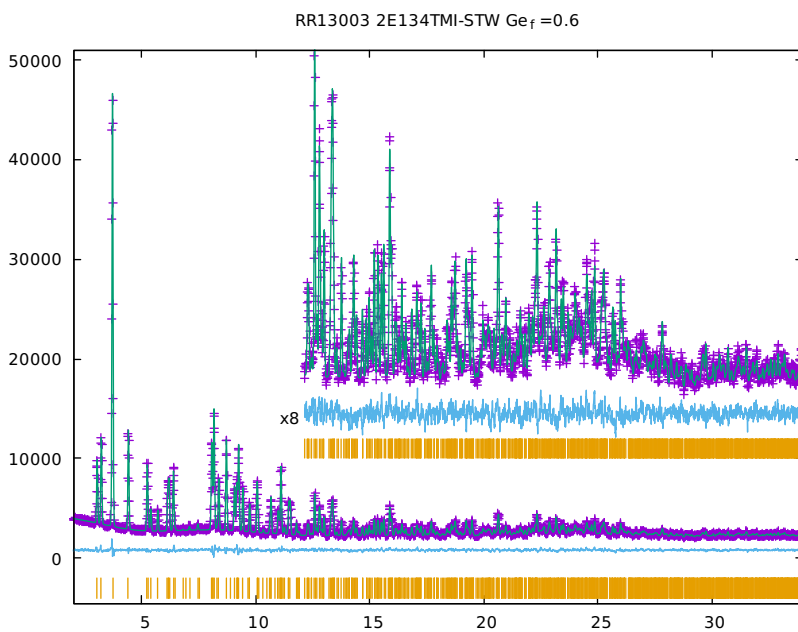


Figure S10. Observed (+) and calculated (solid line) powder X-ray diffractograms for as-made Ge_fSi_{1-f}HPM-1 with $Ge_f = 0.6$ refined in space group $P6_122$. Vertical tic marks indicate the positions of allowed reflections. The lower trace is the difference plot. $\lambda = 0.56383 \text{ \AA}$.

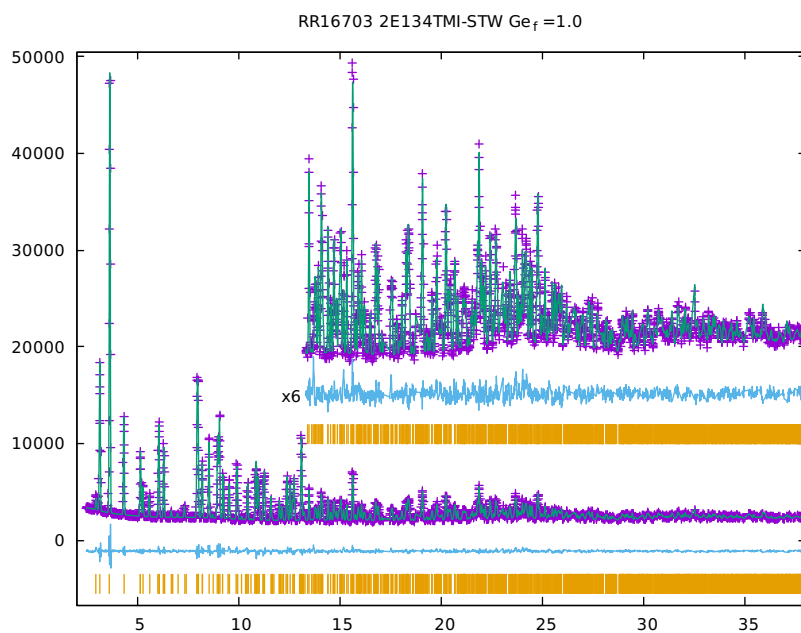


Figure S11. Observed (+) and calculated (solid line) powder X-ray diffractograms for as-made Ge-HPM-1 ($Ge_f = 1.0$) refined in space group $P6_122$. Vertical tic marks indicate the positions of allowed reflections. The lower trace is the difference plot. $\lambda = 0.56383 \text{ \AA}$.

- [1] J. D. Sherman. Synthetic zeolites and other microporous oxide molecular sieves. *Proc. Natl. Acad. Sci. U. S. A.*, 96(7): 3471–3478, 1999.
- [2] Colin S. Cundy and Paul A. Cox. The hydrothermal synthesis of zeolites: History and development from the earliest days to the present time. *Chem. Rev.*, 103(3):663–702, 2003. doi:10.1021/cr020060i.
- [3] Peng Lu, L. A. Villaescusa, and M. A. Cambor. Driving the crystallization of zeolites. *Chem. Rec.*, page 10.1002/tcr.201700092, 2018. ISSN 1528-0691. doi:10.1002/tcr.201700092.
- [4] M. E. Davis and R. F. Lobo. Zeolite and molecular sieve synthesis. *Chem. Mater.*, 4(4):756–768, 1992.
- [5] P. Caullet, J. L. Paillaud, A. Simon-Masseron, M. Soulard, and J. Patarin. The fluoride route: A strategy to crystalline porous materials. *C. R. Chim.*, 8(3-4):245–266, 2005.
- [6] M. A. Cambor and S.B. Hong. *Porous Materials*, pages 265–325. Inorganic Materials Series. Wiley, Chichester, 2011.
- [7] T. Conradsson, M. S. Dadachov, and X. D. Zou. Synthesis and structure of $(\text{Me}_3\text{N})_6[\text{Ge}_{32}\text{O}_{64}] \cdot (\text{H}_2\text{O})_4 \cdot 5$, a thermally stable novel zeotype with 3d interconnected 12-ring channels. *Micropor. Mesopor. Mat.*, 41(1-3):183–191, 2000.
- [8] A. Corma, M. T. Navarro, F. Rey, J. Rius, and S. Valencia. Pure polymorph c of zeolite beta synthesized by using framework isomorphous substitution as a structure-directing mechanism. *Angew. Chem., Int. Ed.*, 40(12):2277–2280, 2001.
- [9] Luis A. Villaescusa and Miguel A. Cambor. The fluoride route to new zeolites. *Recent Res. Dev. Chem.*, 1:93–141, 2003.
- [10] Luis A. Villaescusa and Miguel A. Cambor. Framework reduction of GeO_2 zeolites during calcination. *Chem. Mater.*, 28(20):7544–7550, October 2016.
- [11] Mariya V. Shamzhy, Pavla Eliášová, Dana Vitvarová, Maksym V. Opanasenko, Daniel S. Firth, and Russell E. Morris. Post-synthesis stabilization of germanosilicate zeolites ith, iww, and utl by substitution of ge for al. *Chem.–Eur. J.*, 22(48):17377–17386, 2016. ISSN 1521-3765. doi:10.1002/chem.201603434.
- [12] C. Baerlocher and L. B. McCusker. Database of Zeolite Structures. accessed on March 16th 2018.
- [13] Wieslaw J. Roth, Petr Nachtigall, Russell E. Morris, Paul S. Wheatley, Valerie R. Seymour, Sharon E. Ashbrook, Pavla Chlubná, Lukáš Grajciar, Miroslav Položij, Arnošt Zukal, Oleksiy Shvets, and Jiří Čejka. A family of zeolites with controlled pore size prepared using a top-down method. *Nat Chem*, 5(7):628–633, July 2013. ISSN 1755-4330.
- [14] Pavla Eliášová, Maksym Opanasenko, Paul S. Wheatley, Mariya Shamzhy, Michal Mazur, Petr Nachtigall, Wieslaw J. Roth, Russell E. Morris, and Jiří Čejka. The ador mechanism for the synthesis of new zeolites. *Chem. Soc. Rev.*, 44(3-4): 7177–7206, 2015.
- [15] Paul S. Wheatley, Pavla Chlubná-Eliášová, Heather Greer, Wuzong Zhou, Valerie R. Seymour, Daniel M. Dawson, Sharon E. Ashbrook, Ana B. Pinar, Lynne B. McCusker, Maksym Opanasenko, Jiří Čejka, and Russell E. Morris. Zeolites with continuously tuneable porosity. *Angew. Chem. Int. Ed.*, 53(48):13210–13214, 2014. ISSN 1521-3773. doi: 10.1002/anie.201407676.
- [16] Pavla Chlubná-Eliášová, Yuyang Tian, Ana B. Pinar, Martin Kubo, Jiří Čejka, and Russell E. Morris. The assembly-disassembly-organization-reassembly mechanism for 3d-2d-3d transformation of germanosilicate iww zeolite. *Angew. Chem. Int. Ed.*, 53(27):7048–7052, 2014. ISSN 1521-3773. doi:10.1002/anie.201400600.
- [17] Michal Mazur, Paul S. Wheatley, Marta Navarro, Wieslaw J. Roth, Miroslav Položij, Alvaro Mayoral, Pavla Eliášová, Petr Nachtigall, Jiří Čejka, and Russell E. Morris. Synthesis of ‘unfeasible’ zeolites. *Nat. Chem.*, 8(1):58–62, January 2016.
- [18] Feifei Gao, Maguy Jaber, Krassimir Bozhilov, Aurelie Vicente, Christian Fernandez, and Valentin Valtchev. Framework stabilization of ge-rich zeolites via postsynthesis alumination. *J. Am. Chem. Soc.*, 131(45):16580–16586, November 2009. doi:10.1021/ja904458y.
- [19] Laurence Burel, Nataliia Kasian, and Alain Tuel. Quasi all-silica zeolite obtained by isomorphous degermanation of an as-made germanium-containing precursor. *Angew. Chem. Int. Ed.*, 53(5):1360–1363, 2014. ISSN 1521-3773. doi: 10.1002/anie.201306744.
- [20] Hao Xu, Jin-gang Jiang, Boting Yang, Lin Zhang, Mingyuan He, and Peng Wu. Post-synthesis treatment gives highly stable siliceous zeolites through the isomorphous substitution of silicon for germanium in germanosilicates. *Angew. Chem. Int. Ed.*, 53(5):1355–1359, 2014. ISSN 1521-3773. doi:10.1002/anie.201306527.
- [21] Liqiu Tang, Lei Shi, Charlotte Bonneau, Junliang Sun, Huijuan Yue, Arto Ojuva, Bao-Lin Lee, Mikael Kritikos, Robert G. Bell, Zoltán Bacsik, Janos Mink, and Xiaodong Zou. A zeolite family with chiral and achiral structures built from the same building layer. *Nat. Mater.*, 7(5):381–385, apr 2008. doi:10.1038/nmat2169.
- [22] Alex Rojas and Miguel A. Cambor. A pure silica chiral polymorph with helical pores. *Angew. Chem. Int. Ed.*, 51(16): 3854–3856, 2012. doi:10.1002/anie.201108753.
- [23] Joel E. Schmidt, Michael W. Deem, and Mark E. Davis. Synthesis of a specified, silica molecular sieve by using computationally predicted organic structure-directing agents. *Angew. Chem. Int. Ed.*, 53(32):8372–8374, jun 2014. doi: 10.1002/anie.201404076.
- [24] Stephen K. Brand, Joel E. Schmidt, Michael W. Deem, Frits Daeyaert, Yanhang Ma, Osamu Terasaki, Marat Orazov, and Mark E. Davis. Enantiomerically enriched, polycrystalline molecular sieves. *Proc. Natl. Acad. Sci. U.S.A.*, 114:5101–5106, 2017. doi:10.1073/pnas.1704638114.
- [25] Peng Lu, Luis Gómez-Hortigüela, Lei Xu, and Miguel A. Cambor. Synthesis of stw zeolites using imidazolium-based dications of varying length. *J. Mater. Chem. A*, 6:1485–1495, 2018. doi:10.1039/C7TA10002G.
- [26] Rocio Bueno-Perez, Salvador Rodríguez Gómez Balestra, Miguel A. Cambor, Jung Gi Min, Suk Bong Hong, Patrick J. Merkling, and Sofía Calero. Influence of flexibility on the separation of chiral isomers in the stw-type zeolite. *Chem.–Eur. J.*, 24(16):4121–4132, 1 2018. ISSN 1521-3765. doi:10.1002/chem.201705627.

- [27] Alex Rojas, Oriol Arteaga, Bart Kahr, and Miguel A. Cambor. Synthesis, structure, and optical activity of HPM-1, a pure silica chiral zeolite. *J. Am. Chem. Soc.*, 135(32):11975–11984, aug 2013. doi:10.1021/ja405088c.
- [28] T. J. B. Holland and S. A. T. Redfern. Unit cell refinement from powder diffraction data: The use of regression diagnostics. *Mineral. Mag.*, 61:65–77, 1997. doi:10.1180/minmag.1997.061.404.07.
- [29] A.C. Larson and R.B. Von Dreele. *General Structure Analysis System (GSAS)*. Los Alamos National Laboratory Report LAUR 86-748, 2004.
- [30] B. H. Toby. Expgui, a graphical user interface for gsas. *J. Appl. Crystallogr.*, 34:210–213, 2001.
- [31] Alex Rojas, Luis Gómez-Hortigüela, and Miguel A. Cambor. Zeolite structure direction by simple bis(methylimidazolium) cations: The effect of the spacer length on structure direction and of the imidazolium ring orientation on the 19f NMR resonances. *J. Am. Chem. Soc.*, 134(8):3845–3856, feb 2012. doi:10.1021/ja210703y.
- [32] Jorge Arce-Molina, Ricardo Grau-Crespo, Dewi Wyn Lewis, and A. Rabdel Ruiz-Salvador. Screening heteroatom distributions in zeotype materials using an effective hamiltonian approach: The case of aluminogermanate PKU-9. *Phys. Chem. Chem. Phys.*, 2018. doi:10.1039/c8cp01369a.
- [33] C. R. A. Catlow, M. Dixon, and W. C. Mackrodt. Interionic potentials in ionic solids. In *Computer Simulation of Solids*, pages 130–161. Springer-Verlag, 1982. doi:10.1007/bfb0017937.
- [34] Ricardo Grau-Crespo, Said Hamad, C. R. A. Catlow, and N. H. de Leeuw. Symmetry-adapted configurational modelling of fractional site occupancy in solids. *J. Phys.: Condens. Matter*, 19(25):256201, may 2007. doi:10.1088/0953-8984/19/25/256201.
- [35] Julian D. Gale. Gulp – a computer program for the symmetry adapted simulation of solids. *J. Chem. Soc., Faraday Trans.*, 93:., 1997.
- [36] German Sastre and Julian D. Gale. Derivation of an interatomic potential for germanium- and silicon-containing zeolites and its application to the study of the structures of octadecasil, ASU-7, and ASU-9 materials. *Chem. Mater.*, 15(9):1788–1796, may 2003. doi:10.1021/cm021262y.
- [37] Angeles Pulido, German Sastre, and Avelino Corma. Computational study of 19f NMR spectra of double four ring-containing si/ge-zeolites. *ChemPhysChem*, 7(5):1092–1099, may 2006. doi:10.1002/cphc.200500634.
- [38] Angeles Pulido, Avelino Corma, and German Sastre. Computational study of location and role of fluoride in zeolite structures. *J. Phys. Chem. B*, 110(47):23951–23961, nov 2006. doi:10.1021/jp064278a.
- [39] Paul P Ewald. Die berechnung optischer und elektrostatischer gitterpotentiale. *Ann. Phys.*, 369(3):253–287, 1921.
- [40] William H. Press, Saul A. Teukolsky, William T. Vetterling, and Brian P. Flannery. *Numerical Recipes 3rd Edition: The Art of Scientific Computing*. Cambridge University Press, New York, U.S.A., 3 edition, 2007. ISBN 0521880688, 9780521880688.
- [41] Neyvis Almora-Barrios, A. Rabdel Ruíz-Salvador, Ariel Gómez, Manisha Mistry, and Dewi W. Lewis. Understanding Si/Al distributions in Al-rich zeolites: the role of water in determining the structure of Goosecreekite. *Chem. Commun.*, (6):531–532, 2001. doi:10.1039/b009623g.
- [42] Dewi W. Lewis, A. Rabdel Ruiz-Salvador, Neyvis Almora-Barrios, Ariel Gómez, and Manisha Mistry. Modelling of hydrated ca-rich zeolites. *Mol. Simul.*, 28(6-7):649–661, jun 2002. doi:10.1080/08927020210871.
- [43] Salvador Rodríguez Gómez Balestra, Said Hamad, A. Rabdel Ruíz-Salvador, Virginia Domínguez-García, Patrick J. Merkling, David Dubbeldam, and Sofía Calero. Understanding nanopore window distortions in the reversible molecular valve zeolite RHO. *Chem. Mater.*, 27(16):5657–5667, aug 2015. doi:10.1021/acs.chemmater.5b02103.
- [44] Alex Zunger, S.-H. Wei, L. G. Ferreira, and James E. Bernard. Special quasirandom structures. *Phys. Rev. Lett.*, 65(3):353–356, jul 1990. doi:10.1103/physrevlett.65.353.
- [45] Alexander Urban, Ian Matts, Aziz Abdellahi, and Gerbrand Ceder. Computational design and preparation of cation-disordered oxides for high-energy-density li-ion batteries. *Adv. Energy Mater.*, 6(15):1600488, may 2016. doi:10.1002/aenm.201600488.
- [46] V. Saltas, D. Horlait, E. N. Sgourou, F. Vallianatos, and A. Chroneos. Modelling solid solutions with cluster expansion, special quasirandom structures, and thermodynamic approaches. *Appl. Phys. Rev.*, 4(4):041301, dec 2017. doi:10.1063/1.4999129.
- [47] Chris J. Pickard and Francesco Mauri. All-electron magnetic response with pseudopotentials: NMR chemical shifts. *Phys. Rev. B*, 63(24):245101–1–245101–13, may 2001. doi:10.1103/physrevb.63.245101.
- [48] Jonathan R. Yates, Chris J. Pickard, and Francesco Mauri. Calculation of NMR chemical shifts for extended systems using ultrasoft pseudopotentials. *Phys. Rev. B*, 76(2):024401–1–024401–11, jul 2007. doi:10.1103/physrevb.76.024401.
- [49] John P. Perdew, Kieron Burke, and Matthias Ernzerhof. Generalized gradient approximation made simple. *Phys. Rev. Lett.*, 77:3865–3868, Oct 1996. doi:10.1103/PhysRevLett.77.3865.
- [50] Mickaël Profeta, Magali Benoit, Francesco Mauri, and Chris J. Pickard. First-principles calculation of the ¹⁷O NMR parameters in ca oxide and ca aluminosilicates: the partially covalent nature of the ca-o bond, a challenge for density functional theory. *J. Am. Chem. Soc.*, 126(39):12628–12635, oct 2004. doi:10.1021/ja0490830.
- [51] Aymeric Sadoc, Monique Body, Christophe Legein, Mamata Biswal, Franck Rocquefelte, and Florent Boucher. NMR parameters in alkali, alkaline earth and rare earth fluorides from first principle calculations. *Phys. Chem. Chem. Phys.*, 13(41):18539, 2011. doi:10.1039/c1cp21253b.
- [52] Alfonso Pedone, Thibault Charpentier, and Maria Cristina Menziani. The structure of fluoride-containing bioactive glasses: new insights from first-principles calculations and solid state NMR spectroscopy. *J. Mater. Chem*, 22(25):12599, 2012. doi:10.1039/c2jm30890h.
- [53] Robert Laskowski and Peter Blaha. Origin of NMR shielding in fluorides. *Phys. Rev. B*, 85(24):245117, jun 2012. doi:10.1103/physrevb.85.245117.

- [54] Anmin Zheng, Shang-Bin Liu, and Feng Deng. ^{19}F chemical shift of crystalline metal fluorides: Theoretical predictions based on periodic structure models. *J. Phys. Chem. C*, 113(33):15018–15023, aug 2009. doi:10.1021/jp904454t.
- [55] Charlotte Martineau, Mathieu Allix, Matthew R. Suichomel, Florence Porcher, François Vivet, Christophe Legein, Monique Body, Dominique Massiot, Francis Taulelle, and Franck Fayon. Structure determination of $\text{Ba}_5\text{AlF}_{13}$ by coupling electron, synchrotron and neutron powder diffraction, solid-state NMR and ab initio calculations. *Dalton Trans.*, 45(39):15565–15574, 2016. doi:10.1039/c6dt02454h.
- [56] G. Kresse and J. Hafner. Ab initio molecular dynamics for liquid metals. *Phys. Rev. B*, 47:558–561, 1993. doi:10.1103/PhysRevB.47.558.
- [57] G. Kresse and J. Hafner. Ab initiomolecular-dynamics simulation of the liquid-metal–amorphous-semiconductor transition in germanium. *Phys. Rev. B*, 49(20):14251–14269, may 1994. doi:10.1103/physrevb.49.14251.
- [58] G. Kresse and J. Furthmüller. Efficient iterative schemes for ab initio total-energy calculations using a plane-wave basis set. *Phys. Rev. B*, 54:11169–11186, 1996. doi:10.1103/PhysRevB.54.11169.
- [59] G. Kresse and J. Furthmüller. Efficiency of ab-initio total energy calculations for metals and semiconductors using a plane-wave basis set. *Comput. Mater. Sci.*, 6(1):15–50, jul 1996. doi:10.1016/0927-0256(96)00008-0.
- [60] G. Kresse and D. Joubert. From ultrasoft pseudopotentials to the projector augmented-wave method. *Phys. Rev. B*, 59:1758–1775, 1999. doi:10.1103/PhysRevB.59.1758.
- [61] Stefan Grimme, Jens Antony, Stephan Ehrlich, and Helge Krieg. A consistent and accurate ab initio parametrization of density functional dispersion correction (DFT-d) for the 94 elements h-pu. *J. Chem. Phys.*, 132(15):154104, apr 2010. doi:10.1063/1.3382344.
- [62] Na Zhang, Lei Shi, Tingting Yu, Tianduo Li, Wei Hua, and Cong Lin. Synthesis and characterization of pure STW-zeolite germanosilicate, cu- and co-substituted STW-zeolite materials. *J. Solid State Chem.*, 225:271–277, may 2015. doi:10.1016/j.jssc.2014.12.031.
- [63] J. Dwyer and K. Karim. The incorporation of heteroatoms into faujastic framework by secondary synthesis using aqueous fluoride complexes. *J. Chem. Soc., Chem. Commun.*, (14):905, 1991. doi:10.1039/c39910000905.
- [64] Miguel A. Camblor, Avelino Corma, Agustín Martínez, and Joaquín Pérez-Pariente. Synthesis of a titaniumsilicoaluminate isomorphous to zeolite beta and its application as a catalyst for the selective oxidation of large organic molecules. *J. Chem. Soc., Chem. Commun.*, 0(8):589–590, 1992. doi:10.1039/c39920000589.
- [65] B. Sulikowski. Isomorphous replacement in the zeolitic frameworks: Recent advances and implications. *Heterog. Chem. Rev.*, (3):203–268, 1996.
- [66] Miguel A. Camblor, Suk Bong Hong, and Mark E. Davis. Unexpected contraction of a zeolite framework upon isomorphous substitution of si by al. *Chem. Commun.*, (3):425, 1996. doi:10.1039/cc9960000425.
- [67] H. Kosslick, V. A. Tuan, R. Fricke, C. Peuker, W. Pilz, and W. Storek. Synthesis and characterization of Ge-ZSM-5 zeolites. *J. Phys. Chem.*, 97(21):5678–5684, may 1993. doi:10.1021/j100123a036.
- [68] E. Verheyen, L. Joos, C. Martineau, C. J. Dawson, C. Weidenthaler, W. Schmidt, R. Yuan, E. Breynaert, V. Van Speybroeck, M. Waroquier, F. Taulelle, M. M. J. Treacy, J. A. Martens, and C. E. A. Kirschhock. Flexibility versus rigidity: what determines the stability of zeolite frameworks? a case study. *Mater. Horiz.*, 1(6):582–587, 2014. doi:10.1039/c4mh00127c.
- [69] Juan José Gutiérrez-Sevillano, Sofía Calero, Said Hamad, Ricardo Grau-Crespo, Fernando Rey, Susana Valencia, Miguel Palomino, Salvador Rodríguez Gómez Balestra, and A. Rabdel Ruíz-Salvador. Critical role of dynamic flexibility in ge-containing zeolites: Impact on diffusion. *Chem.–Eur. J.*, 22(29):10036–10043, jun 2016. doi:10.1002/chem.201600983.
- [70] Joel E. Schmidt, Stacey I. Zones, Dan Xie, and Mark E. Davis. The synthesis of aluminophosphate and germanosilicate lta using a triquaternary structure directing agent. *Micropor. Mesopor. Mat.*, 200:132–139, December 2014.
- [71] Sarah R. Whittleton, Aurelie Vicente, Christian Fernandez, Somayeh F. Rastegar, Anna V. Fishchuk, and Stepan Sklenak. Effect of ge/si substitutions on the local geometry of si framework sites in zeolites: A combined high resolution 29 si MAS NMR and DFT/MM study on zeolite beta polymorph c (BEC). *Micropor. Mesopor. Mat.*, 267:124–133, sep 2018. doi:10.1016/j.micromeso.2018.03.021.
- [72] Po Caultet, JL Guth, J Hazm, JM Lamblin, and H Gies. Synthesis, characterization and crystal-structure of the new clathrasil phase octadecasil. *Eur. J. Sol. State Inor.*, 22(28):345–361, 1991.
- [73] Luis A. Villaescusa, Philip A. Barrett, and Miguel A. Camblor. Itq-7: A new pure silica polymorph with a three-dimensional system of large pore channels. *Angew. Chem. Int. Ed.*, 38(13-14):1997–2000, 1999. ISSN 1521-3773. doi:10.1002/(SICI)1521-3773(19990712)38:13/14<1997::AID-ANIE1997>3.0.CO;2-U.
- [74] Miguel A. Camblor, Philip A. Barrett, María José Díaz-Cabañas, Luis A. Villaescusa, Marta Puche, Teresa Boix, Eva Pérez, and Hubert Koller. High silica zeolites with three-dimensional systems of large pore channels. *Micropor. Mesopor. Mat.*, 48(1-3):11–22, nov 2001. doi:10.1016/s1387-1811(01)00325-0.
- [75] Philip A. Barrett, Teresa Boix, Marta Puche, David H. Olson, Edgar Jordan, Hubert Koller, and Miguel A. Camblor. ITQ-12: a new microporous silica polymorph potentially useful for light hydrocarbon separations. *Chem. Commun.*, (17):2114, 2003. doi:10.1039/b306440a.
- [76] Luis A. Villaescusa, Philip Lightfoot, and Russell E. Morris. Synthesis and structure of fluoride-containing GeO_2 analogues of zeolite double four-ring building units. *Chem. Commun.*, (19):2220–2221, sep 2002. doi:10.1039/b207374a.
- [77] German Sastre, Jose A. Vidal-Moya, Teresa Blasco, Jordi Rius, Jose L. Jordá, Maria T. Navarro, Fernando Rey, and Avelino Corma. Preferential location of ge atoms in polymorph c of beta zeolite (ITQ-17) and their structure-directing effect: A computational, XRD, and NMR spectroscopic study. *Angew. Chem. Int. Ed.*, 41(24):4722–4726, dec 2002. doi:10.1002/anie.200290028.
- [78] Teresa Blasco, Avelino Corma, M José Díaz-Cabañas, Fernando Rey, José A. Vidal-Moya, and Claudio M. Zicovich-Wilson. Preferential location of ge in the double four-membered ring units of ITQ-7 zeolite. *J. Phys. Chem. B*, 106(10):2634–2642,

mar 2002. doi:10.1021/jp013302b.

- [79] K. Wang, J. Yu, C. Li, and R. Xu. Investigation on the chain-to-chain and chain-to-open-framework transformations of two one-dimensional aluminophosphate chains. *Inorg. Chem.*, 42:4597–4602, 2003.
- [80] Yingxia Wang, Jiaqing Song, and Hermann Gies. The substitution of germanium for silicon in AST-type zeolite. *Solid State Sci.*, 5(11-12):1421–1433, nov 2003. doi:10.1016/j.solidstatesciences.2003.09.003.
- [81] Luis A. Villaescusa and Miguel A. Cambor. Time evolution of an aluminogermanate zeolite synthesis: Segregation of two closely similar phases with the same structure type. *Chem. Mater.*, 28(9):3090–3098, may 2016. doi:10.1021/acs.chemmater.6b00507.
- [82] German Sastre, Angel Cantin, Maria Jose Díaz-Cabañas, and Avelino Corma. Searching organic structure directing agents for the synthesis of specific zeolitic structures: an experimentally tested computational study. *Chem. Mater.*, 17(3): 545–552, feb 2005. doi:10.1021/cm049912g.